Systematic Investigation of Modern Quantum Chemical Methods to Predict Electronic Circular Dichroism Spectra

Christian Diedrich and Stefan Grimme*

Theoretische Organische Chemie, Organisch-Chemisches Institut der Universität Münster, Corrensstrasse 40, D-48149 Münster, Germany

Received: November 28, 2002; In Final Form: February 11, 2003

The ability of different quantum chemical methods to predict experimental electronic circular dichroism (CD) spectra is critically evaluated. Two single-reference, time-dependent approaches based either on density functional theory (TDDFT) or a simplified coupled-cluster expansion (CC2) and two multireference methods (MRMP2 and DFT/MRCI) are considered. The methods are applied to a test suite of seven molecules including a wide range of difficult chromophores ("real-life" examples) and to three model systems—H_2S_2, twisted ethylene, and dimethyloxirane—where accurate ab initio MRCI reference data are used for comparison. To investigate the effect of "exact" exchange mixing systematically, the TDDFT calculations were carried out with the BP86, B3-LYP, and BH-LYP functionals. The time-dependent Hartree−Fock (TDHF) method was included as an "upper limit" for the HF-exchange part in the functional. In general, it is found that the accuracy of most of the simulated spectra (except those from TDHF) is good enough to assign absolute configurations of chiral molecules with very high certainty. However, the description of weakly disturbed, inherently achiral chromophores and systems with Rydberg−valence mixing turned out to be rather difficult. Furthermore, none of the methods perform reliably for all of the molecules in the test suite, and in particular, the TDDFT results are very sensitive to the functional used. The best overall performance is achieved with the DFT/MRCI and CC2 methods. The TDDFT method should be used carefully, especially for systems with important diffuse or charge-transfer states. Out of the three functionals tested, B3-LYP seems to perform best. In practice, we highly recommend the simultaneous application of different complementary single and multireference methods, which significantly increases the reliability of theoretical predictions.

1. Introduction

The optical properties of chiral molecules are of fundamental interest in chemistry and biochemistry. The main perspective of so-called "structure−chiroptic" relationships is their ability to determine the absolute configuration of chiral substances, which is of particular importance for compounds with pharmacological relevance. One of the most widely used methods in chiral spectroscopy is electronic circular dichroism (CD) where the difference of the absorption coefficients for left and right circularly polarized light ($\Delta\epsilon$) is measured.[1−3] Because CD signals can be positive or negative, an additional "dimension" compared to the dimensionality of conventional UV/vis spectroscopy is introduced into these spectra, which makes CD spectroscopy relatively sensitive to details of the geometric and electronic structures of molecules.

Although several semiempirical structure−chiroptic rules[4−6] have been suggested successfully in the past, it is clear that an exploration of the full potential of the CD method in general requires an accurate theoretical treatment. The first relatively extensive theoretical study of the CD of larger molecules obtained with quantum chemical methods based on modern density functional theory (DFT) appeared in 1998.[7] Since then, these[8−10] and other methods[11] have been developed further, and thus it seems appropriate to investigate their performance in calculating electronic CD in detail.

The main quantity in CD spectroscopy is the rotatory strength determining the intensity of an absorption band ranging from wavelengths λ_1 to λ_2 given (in cgs units) by

$$R = 2.297 \times 10^{-39} \int_{\lambda_1}^{\lambda_2} \frac{\Delta\epsilon(\lambda)}{\lambda}\, d\lambda \tag{1}$$

For a transition between states $|\Psi_0\rangle$ and $|\Psi_i\rangle$, it is theoretically defined as

$$\begin{aligned} R_{0i} &= Im(\langle\Psi_0|\hat{\mu}|\Psi_i\rangle\langle\Psi_0|\hat{m}|\Psi_i\rangle) \\ &= |\vec{\mu_{0i}}|\cdot|\vec{m_{0i}}|\cdot\cos(\vec{\mu_{0i}}, \vec{m_{0i}}). \end{aligned} \tag{2}$$

Here, $\hat{\mu}$ and $\hat{m}$ are the electric and magnetic dipole operators, respectively. An inspection of eq 2 shows that the electric and magnetic transition dipole moments $\vec{\mu_{01}}$ and $\vec{m_{0i}}$ as well as the angle between both moments have to be determined. Therefore, an accurate prediction of rotatory strengths represents a significantly more demanding task than the calculation of oscillator strengths. Furthermore, because rotatory strengths are signed quantities, the excitation energies must be known with higher accuracy than in UV/vis spectroscopy to avoid an incorrect cancellation of neighboring bands with opposite sign. CD spectroscopy naturally deals with systems of relatively low symmetry (typically the C_2 point group), and in practice, a large number of excited states are required to simulate CD spectra over the entire wavelength range that is usually measured (200−700 nm). Even if we do not consider the inherent problems with an accurate quantum chemical description of excited states (as compared to ground states) in general, it is clear that the theoretical simulation of CD spectra is a formidable task.

* Corresponding author. E-mail: grimmes@uni-muenster.de.

10.1021/jp0275802 CCC: $25.00
Published on Web 03/18/2003

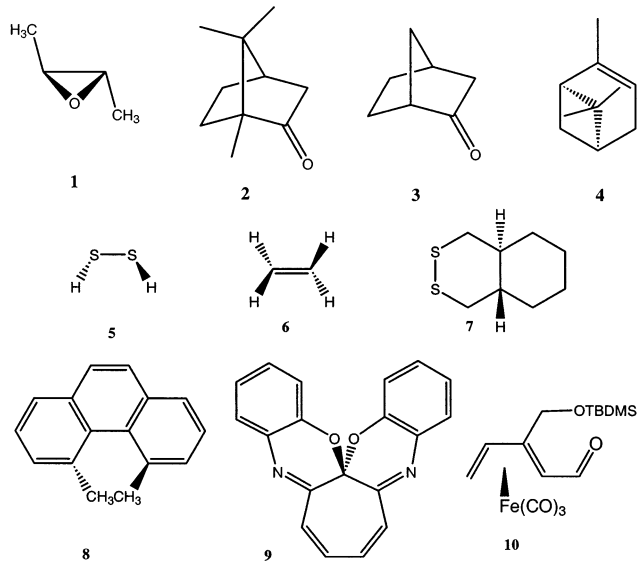

Figure 1. Investigated molecules with inherently achiral (**1**−**4**) and chiral (**5**−**10**) chromophores.

The major aim of this work is to evaluate the performance of today's state-of-the-art quantum chemical methods to reproduce experimental CD spectra. Our investigation includes the time-dependent (single-reference) Hartree−Fock (TDHF) and density functional theory (TDDFT)[12] methods and a coupled-cluster model including single and approximate double excitations (CC2).[13] The second group of methods is based on a multireference treatment either ab initio using perturbation theory (MRMP2[14]) or variational in combination with DFT (called DFT/MRCI[15]). This study continues and extends our previous investigation[16] of a variety of different chromophores with TDDFT, CC2, and MRMP2 methods that was, however, restricted to excitation energies and low-lying excited states.

Because of the known drawbacks of current implementations of TDDFT[17] with respect to a balanced description of valence and Rydberg excited states and general difficulties with charge-transfer transitions (see refs 18 and 19 for suggestions to solve this problems), three functionals (BP86, B3-LYP, and BH-LYP) with an increasing fraction of "exact" exchange (HFXC) in the functional (0, 20, and 50%, respectively) have been employed. This enables a systematic investigation of problems related to the wrong asymptotic form (see, for example, ref 20) of most current DF potentials.

The different methods have been applied to a carefully chosen test suite of molecules (see Figure 1) that may be used as a "benchmark set" in future investigations. The molecules have been chosen to provide a wide range of chromophores (from C_2H_4 to a tricarbonyl−pentadienal−iron complex) with general importance in CD spectroscopy, with conformational rigidity and the availability of good experimental data used as preconditions. The concept of the chromophore, its local symmetry, and the "surroundings" (substituents) plays an important role in CD spectroscopy. If the chromophore itself is chiral, it is denoted as "inherently chiral", and typically intensive Cotton effects are observed. In these cases, the study of model compounds can be helpful for understanding the electronic properties of the system or for calibration purposes. In the second (larger) group of molecules, the chromophore is locally achiral but is disturbed by its chiral surrounding (inherently achiral chromophore), and much weaker Cotton effects (1 to 2 orders of magnitude) are usually observed.

Carbonyl groups and isolated double bonds appear in many natural products and are therefore important examples of inherently achiral chromophores. The corresponding compounds in our test suite are two camphor derivatives (camphor and norcamphor) and the terpene (−)-α-pinene. Possibly the most prominent examples of inherently chiral chromophores are helicenes. Much effort has been put into the investigation of such screw-shaped molecules,[7,21−23] and they have contributed significantly to our understanding of CD. In this work, we consider the helicene derivative 4,5-dimethylphenanthrene and, as an example of a natural molecule with a distorted delocalized π system, the troponoid spiro compound (*S*)-cyclohepta[1,2-b:1,7-b′]bis[1,4]-benzoxazine (CBB). According to its importance to the secondary and tertiary structures of peptides, we include (*S*,*S*)-dithiadecaline in the second group. Before considering these "real" systems, three small model compounds (dimethyloxirane, dihydrogendisulfide, and twisted ethylene) are investigated. In these cases, large MRCI calculations that provide accurate reference data for the other more approximate approaches have been carried out.

The paper is organized as follows: The computational details are given in section 2. Results and Discussion (section 3) is divided into two parts: (1) the results for the model compounds and (2) the results concerned with the real systems. For each system, a short overview is given first. The presentation of the results is divided into a discussion of the excitation energies and rotatory strengths obtained with the different methods and a comparison of the theoretical and experimental CD spectra. A general conclusion about the performance and applicability of the different methods to the problem finalizes our work.

2. Computational Details

All SCF and response theory calculations have been carried out with the TURBOMOLE suite of programs.[24] The program modules escf[17] and cc2[25] have been used in the TDDFT and coupled-cluster (CC2) response treatments. Unfortunately, the current CC2 implementation does not allow a determination of the configuration contributions to a given transition to be made. Therefore, the assignments of the transitions are based on energy and transition moments in this case and are thus less reliable than for the other methods. For the MRMP2, DFT/MRCI, and MRCI calculations, the program packages rimr[14] and mrci[15] that were developed in our laboratory have been employed.

All ground-state geometries have been optimized at the DFT/B3-LYP level by employing a Gaussian AO basis set of valence triple-ζ quality augmented with polarization functions on all atoms (TZVP[26]). The ethylene and dihydrogendisulfide model geometries have been obtained by adjusting the respective dihedral angles after optimization. If not stated otherwise, split-valence basis sets SV(P) with polarization functions on all but the hydrogen atoms[27] have been used throughout this study. All results have been compared to TZVP calculations, and if significant deviations are observed, results with the larger basis set are presented. This procedure was chosen according to the basic intention of this work to evaluate the applicability of the methods to large systems where extended basis sets may be prohibitive in terms of computation time. Diffuse basis functions (taken from the aug-cc-pVTZ basis sets of Dunning[28,29]) have been added to all atoms in cases where Rydberg states are important (ethylene, dimethyloxirane, the camphor derivatives, pinene, H_2S_2, dithiadecaline). This procedure is not generally applicable in the case of the MRMP2 method, where large virtual orbital spaces sometimes cause a breakdown of the perturbation series.[30] Therefore, in this case, a single uncontracted set of diffuse functions (s exponents: 0.08, 0.04, 0.02, 0.01; p exponents: 0.08, 0.04, 0.02, 0.01; d exponents: 0.04,

0.02, 0.01) is placed at the center of charge (as obtained by a ROHF calculation) of the corresponding cation.

In all MRMP2 calculations, we used "half-electron" cation SCF orbitals (two half-electrons in the HOMO) to improve the virtual Hartree−Fock orbitals. This procedure has the advantage over standard ROHF cation orbitals that it can be extended to cases such as the disulfide chromophore where the low-lying transitions result from two different orbitals. In that case, we generate orbitals with an occupation of 1.5e in each orbital to obtain an "average over the two cations".

The Coulomb operator in the DFT/BP86 calculations was approximated by the resolution of the identity (RI) technique[31] using the auxiliary basis sets from the TURBOMOLE library.[32] The RI approximation was also used in the CC2, MRMP2, and DFT/MRCI calculations where MP2-optimized auxiliary basis sets have been employed.[33] According to a large body of experience, the errors due to the RI approximation are less than 0.03 eV for the excitation energies.

As reference wave functions in the MRMP2 treatments, excitation-level restricted CI wave functions in a selected space of orbitals (RAS) have been employed. The RAS has been iteratively generated as described in ref 16. The MRMP2 first-order space has been truncated by a configuration selection procedure[34] based on a diagonal approximation. The $T_{sel} = 0.1\mu E_h$ selector threshold[14] for the model compounds and $0.5\mu E_h$ for the real systems have been used, respectively. Except for ethylene, in all MRMP2 calculations a level shift[35] of $0.2E_h$ is necessary to avoid intruder states. The one-electron (transition) properties were calculated as expectation values of the first-order corrected MRMP2 wave functions. The MRCI expansions were also truncated by (diagonal) MRMP2 configuration selection (for the applied thresholds; see section 3.1) and subsequent addition of the discarded MRMP2 energy contributions to the variational CI energy. The Davidson correction[36] has been employed to compensate approximately for the size inconsistency of the CI method. The DFT/MRCI calculations, which always use the BH-LYP functional, were performed as described in detail in ref 15 using a configuration selection cutoff of $0.8E_h$. Without any significant loss of accuracy, this leads to drastic savings in computational cost compared to the suggested value of $1.0E_h$.[15]

All excited-state calculations have been performed at the ground-state geometries. The results correspond thus to vertical transitions, and the excitation energies can be approximately identified as the band maxima in the experimental spectra. In the DFT/MRCI, MRMP2, and CC2 calculations, all core electrons were excluded from the correlation treatment whereas the full singles expansion space was considered within the TDDFT/TDHF approaches.

The rotatory strengths can be calculated either in the dipole length or the dipole velocity formalism depending on which expression for the electric perturbation is inserted into eq 2:

$$R_{0i}^{r} = \frac{1}{2c}\langle\Psi_0|\hat{r}\times\hat{\nabla}|\Psi_i\rangle\langle\Psi_0|\hat{r}|\Psi_i\rangle \qquad (3)$$

$$R_{0i}^{\nabla} = \frac{1}{2cE_{0i}}\langle\Psi_0|\hat{r}\times\hat{\nabla}|\Psi_i\rangle\langle\Psi_0|\hat{\nabla}|\Psi_i\rangle$$

The velocity form (R^{∇}) is gauche invariant but relatively sensitive to the quality of the wave function. The length form (R^{r}) is origin-dependent but provides a higher robustness and according to our experience yields better results in most cases. Hence, it is used throughout this work, although R^{∇} has always been calculated as a check.

The CD spectra were simulated by overlapping Gaussian functions for each transition according to

$$\Delta\epsilon(E) = \frac{1}{2.297\times10^{-39}}\frac{1}{\sqrt{2\pi}\sigma}\sum_{i}^{A}\Delta E_i R_i e^{[-(E-\Delta E_i/2\sigma)]^2} \qquad (4)$$

where σ is the width of the band at $^1/_e$ height and ΔE_i and R_i are the excitation energies and rotatory strengths for transition i, respectively. If not stated otherwise, a σ value of 0.2 eV was used.

3. Results and Discussion

3.1. Model Compounds. 3.1.1. (*M*)-H_2S_2 (5). The chiroptical properties of the disulfide chromophore have been the subject of many experimental and theoretical studies.[37−39] The main focus of these works was the CD dependence on the dihedral angle ϕ^{RSSR} (angle of heliticity). A semiempirical explanation for this dependence was given by Linderberg and Michl.[40] On the basis of the Bergson model,[41,42] they predicted a positive sign for the first transition in right-handed disulfide groups if ϕ^{RSSR} is less than 90° and vice versa. This follows from the crossing of two electronic states of A and B symmetry (in C_2) related to transitions with oppositely signed rotatory strengths. In the Koopman's picture, this refers to a crossing of the 8b and 9a orbitals arising from the π-bonding character of the latter with $\phi^{RSSR} > 90°$ and the π antibonding character with $\phi^{RSSR} < 90°$ whereas the opposite holds for the 8b orbital. The disulfide compounds investigated in this work, namely, 2,3-(*S*,*S*)-dithiadecaline and (*M*)-H_2S_2, have a ϕ^{RSSR} value of −56.5°; therefore, the Cotton effect of the first band is negative for the considered left-handed enantiomer. Taking the z axis as the 2-fold axis of rotation, totally symmetric A transitions are electrically and magnetically polarized along this axis whereas B-type excitations are polarized perpendicular to z in the x, y plane.

Typical for chromophors containing sulfur is that all of the low-lying transitions exhibit Rydberg contributions to a certain extent. The eight first excited states of H_2S_2 can roughly be divided into five valence states with varying Rydberg contributions and three Rydberg states with varying valence contributions. To account for this Rydberg−valence mixing, all calculations have been carried out using a triple-ζ basis set augmented with (2d1f) polarization and diffuse functions[43](aug-TZVPP).

Results. The small size of the H_2S_2 molecule (14 correlated electrons) permits an accurate MRCI treatment. These results (Table 1) were obtained at the CI level including about 1.3×10^6 configurations ($T_{sel} = 0.025\mu E_h$) that can be considered to be quite close to the AO basis set limit. If the size of the AO basis set is reduced (S: aug-TZVPP; H: TZVP), then the second and third transitions are interchanged, indicating the sensitivity of the system. The Rydberg−valence mixing is reflected by the $\Delta\langle r^2\rangle$ values (difference between the $\langle r^2\rangle$ expectation values of the ground state and the excited state; typical values for pure valence excitations are close to zero whereas pure Rydberg states show $\langle r^2\rangle$ values between 30 and 50 a_0^2) that are, for example, about 15 a_0^2 for the $n_x \rightarrow \sigma(SH)^*$ states.

The excitation energies in Table 1 are shifted with respect to the MRCI excitation energy for the $n_a \rightarrow \sigma(SS)^*$ transition to account for systematic errors and to simplify the comparison of the methods. The ordering of the considered states is correctly reproduced by all methods, but TDDFT/BP86 predicts an $n_b \rightarrow \sigma(SH)_2^*$ (not shown in Table 1) transition slightly below the $n_a \rightarrow 3p_z$ transition. For the TDDFT/TDHF methods, a

TABLE 1: Excitation Energies (eV) and Rotatory Strengths (10^{-40} cgs units) for H_2S_2 (5)

state/classification	$\Delta E/R^r$	TDHF	TDDFT BH-LYP	TDDFT B3-LYP	TDDFT BP86	CC2	DFT/MRCI	MRMP2[a]	MRCI
1B	ΔE	4.00	4.00	4.00	4.00	4.00	4.00	4.00	4.00
$n_a \rightarrow \sigma(SS)^*$	R^r	−9.7	−7.4	−6.3	−4.9	−6.6	−7.6	−8.6	−8.2
2A	ΔE	5.24	5.20	5.04	5.00	5.11	5.10	5.26	5.16
$n_a \rightarrow \sigma(SH)_1^*$	R^r	−5.0	−7.5	−13.3	−14.1	−17.8	−6.8	−30.5	−15.1
3A	ΔE	5.73	5.51	5.36	5.30	5.48	5.36	5.34	5.37
$n_b \rightarrow \sigma(SS)^*$	R^r	*−7.5*	0.2	8.8	12.7	6.4	2.2	15.4	3.4
2B	ΔE	6.23	6.21	6.08	6.03	6.20	6.12	6.29	6.23
$n_a \rightarrow \sigma(SH)_2^*$	R^r	*3.2*	−8.1	−29.9	−51.2	−11.6	−10.3	−12.3	−5.6
3B	ΔE	7.54[c]	7.02	6.50	6.34	6.77	6.73	6.73	6.81
$n_b \rightarrow \sigma(SH)_1^*$	R^r	52.1[c]	32.2	46.4	64.2	41.8	27.0	52.5	35.5
4A	ΔE	7.45	7.30	7.00	6.90	7.21	7.31	7.39	7.30
$n_a \rightarrow 3s$	R^r	−11.5	−7.0	−4.1	−5.1	−3.8	−17.5	−0.5	−4.1
5A	ΔE	7.67	7.51	7.28	7.35[d]	7.45	7.59	7.65	7.54
$n_a \rightarrow 3p_z$	R^r	−22.6	−21.5	−17.6	−2.7[d]	−25.0	−23.3	−16.8	−21.8
4B	ΔE	7.70	7.67	7.43	7.43	7.56	7.70	7.75	7.70
$n_a \rightarrow 3p_1$	R^r	16.7	19.1	12.9	15.2	17.8	19.6	14.1	14.9
shift value (eV)[b]		−0.39	0.01	0.26	0.38	−0.08	0.25	0.13	
MAD[e]	ΔE	0.12[g]	0.07	0.20	0.25	0.08	0.05	0.07	
MRD[f]	R^r	111%[g]	39%	86%	166%	36%	72%	93%	

[a] Calculation performed with HF(N-1) orbitals; see section 2 for details. [b] Shifts with respect to MRCI energy for the $n_a \rightarrow \sigma(SS)^*$ transition; positive values indicate that the calculated excitation energies are too low. [c] Strong mixing; classification not possible. [d] TDDFT/BP86 predicts a $n_b \rightarrow \sigma(SH)_2^*$ transition slightly below. [e] Corresponds to the shifted excitation energies. The reference value was excluded. [f] Mean relative deviation. [g] 3B state excluded.

dependence of the systematic errors on the fraction of HFXC is observed. With TDHF (100% HF exchange), the well-known systematic overestimation of all excitation energies is found (shift of −0.39 eV) whereas TDDFT/BP86 predicts values that are much too low (shift of 0.38 eV). According to their HF-exchange fraction, the hybrid functionals B3-LYP and BH-LYP interpolate more or less linearly between the HF and BP86 extremes. The best results are achieved with the BH-LYP functional (shift of 0.01 eV). Similar behavior of the functionals is also observed for the other systems treated in this work, although we emphasize that, unfortunately, the optimal fraction of HFXC is not constant but differs in an unpredictable fashion. If one is interested in spectral simulations, however, a more serious problem than the systematic shifts is the unbalanced description of states with different spatial dimensions as observed for the TDDFT calculations with the BP86 and B3-LYP functionals. This effect is mainly due to the incorrect asymptotic behavior of the exchange correlation functionals,[20] leading to an underestimation of Rydberg excitation energies. An increase of HFXC circumvents this problem to some extent. This results in decreasing the mean abolute deviation (MAD), which is lowest for TDDFT/BH-LYP. The DFT/MRCI method yields comparable or better (for the 3A and the 3B state) results. The energies predicted by CC2 and MRMP2 nicely agree with the MRCI reference values. Even on an absolute scale, the errors are within 0.1−0.2 eV.

Again, taking the MRCI values as a reference, all methods (except TDHF for the $n_b \rightarrow \sigma(SS)^*$ transition) correctly predict the signs of the rotatory strengths, but the agreement of the absolute values is not satisfying. For the HOMO → LUMO (1B) and the "pure" Rydberg transitions (4A, 5A, 4B), the performance of the approximate methods is slightly better than for the remaining transitions. This probably reflects the strong Rydberg−valence mixing of the latter ($\Delta\langle\hat{r}^2\rangle$ values between 7.7 and $19.9a_0^2$). For most of the transitions, the rotatory strengths obtained from the TDDFT/TDHF calculations suffer from an unpredictable dependence on the amount of "exact" exchange mixing. The rotatory strengths of the electronically very different transitions HOMO → LUMO and $n_a \rightarrow 3p_{z/1}$, for example, decrease with decreasing HFXC whereas the opposite is true for the 2A−3B states. The strongest dependency is found for the $n_a \rightarrow \sigma(SH)_2^*$ transition, where TDHF predicts the wrong sign (+3.21), whereas TDDFT/BP86 predicts the right sign but overestimates the absolute value by a factor of 9. The mean relative deviations ($MRD = \sum_i^N (100|(R_{ref} - R)/R_{ref}|)/N$) of the TDDFT methods indicate that (similar to the excitation energies) the best results are obtained with the BH-LYP functional. The significantly larger MRD from the DFT/MRCI method is mainly due to the $n_a \rightarrow 3s$ transition. The remaining values are of similar quality. The best agreement is achieved with the CC2 method (MRD: 36%). The MRMP2 method overestimates the Cotton effects for the transitions leading to $\sigma(SH)^*$-type excited states and for the $n_b \rightarrow \sigma(SS)^*$ transition. As mentioned before, these states exhibit the strongest Rydberg−valence mixing and are therefore very difficult to treat perturbatively. In summary, we observe a large discrepancy between the relatively well reproduced excitation energies and partially strong deviations for the rotatory strengths. This finding confirms our previous analysis that the theoretical predictions of rotatory strengths are significantly more demanding than those of excitation energies. Obviously, in some cases, good results for the latter are due to error compensation rather than an appropriate description of the corresponding wave functions. Nevertheless, the promising results obtained with the TDDFT/BH-LYP and DFT/MRCI methods indicate that the application of hybrid functionals significantly improves performance, especially for diffuse excited states, and thereby leads to better results for the transition moments.

3.1.2. (*M*)-Ethylene (6). Considering the difficulties with Rydberg−valence mixed excitations observed for H_2S_2, further investigation of such transitions in another system seems

TABLE 2: Excitation Energies (eV) and Rotatory Strengths (10^{-40} cgs units) for −10° Twisted Ethylene (6)

state/classification	$\Delta E/R^r$	TDHF	TDDFT BH-LYP	TDDFT B3-LYP	TDDFT BP86[c]	CC2	DFT/MRCI	MRMP2[a]	MRCI
$1B_3$	ΔE	7.19	7.19	7.19	7.19	7.19	7.19	7.19	7.19
$\pi \rightarrow 3s$	R^r	27.8	27.2	25.8	26.2	30.6	31.2	25.3	26.2
$1B_1$	ΔE	7.35	7.55	7.78	7.72	7.76	7.54	7.68	7.78
$\pi \rightarrow \pi^*$	R^r	98.4	136.6	163.0	158.1	163.8	197.8	116.8	74.9
$2B_1$	ΔE	7.80	7.79	7.77	7.74	7.86	7.91	7.88	7.89
$\pi \rightarrow 3p_y$	R^r	3.5	4.9	2.8	30.1	−0.2	6.5	2.3	2.3
$1B_2$	ΔE	7.97	7.86	7.76	7.70	7.89	7.85	7.91	7.91
$\pi \rightarrow 3p_z$	R^r	−0.9	−0.6	−0.4	−0.8	−1.4	−1.2	−0.8	−0.1
$2B_3$	ΔE	9.24	9.18	9.17	9.20	9.20	9.26	9.20	9.20
$\pi \rightarrow 3d_{x^2-y^2}$	R^r	9.3	8.4	10.2	14.7	9.0	7.4	8.5	7.2
shift value (eV)[b]		0.07	0.26	0.60	0.59	0.03	0.31	−0.02	
MAD[d]	ΔE	0.16	0.10	0.08	0.11	0.02	0.10	0.03	
MRD[e]	R^r	30%	54%	46%	356%	67%	92%	19%	

[a] Calculation performed with HF(N-1) orbitals. [b] Shifts with respect to MRCI energy for the p → 3s transition; positive values indicate that the calculated excitation energies are too low. [c] In contrast to all other methods, TDDFT/BP86 predicts a σ(SH) → 3s transition at $\Delta E = 9.13$ eV. [d] Corresponds to the shifted excitation energies. The reference value was excluded. [e] Mean relative deviation; the $1B_2$ state was excluded because of the very small reference value.

appropriate. One of the simplest examples for a chiral molecule with Rydberg−valence mixing is the twisted ethylene molecule. It has been extensively investigated as a model compound for strained cyclic monoenes such as *trans*-cyclooctene.[44,45] For the sake of consistency with previous work, a double-bond torsion angle of −10° has been used.

The twisted ethylene molecule belongs to the D_2 point group. Therefore, all totally symmetric transitions are electric and magnetic dipole-forbidden whereas those leading to states of B_1, B_2, or B_3 symmetry are characterized by parallel or antiparallel vectors of the electric and magnetic transition dipole moments. The absolute value of the rotatory strength is then simply given by the product of the norms of both vectors (eq 2). The calculations have been restricted to the first five electric dipole-allowed transitions.

Results. All calculations have been performed by employing the TZVP basis set augmented with diffuse functions (aug) on all atoms. According to MRCI studies with different basis sets (aug-SV(P), aug-TZVP, aug-TZVPP), aug-TZVP provides accurate results for this system. The MRCI reference calculation was carried out using a threshold of $10^{-4}\mu E_h$ in the configuration selection procedure (section 2), yielding 2.6×10^6 configurations. The $\Delta\langle r^2\rangle$ value of the $\pi \rightarrow \pi^*$ state ($11.5a_0^2$, MRCI/aug-TZVP) reflects its Rydberg−valence mixed character. Nevertheless, the large oscillator strength of $f^r = 0.3251$ indicates that the valence character dominates.

The ΔE values in Table 2 have been shifted with respect to the MRCI result for the $\pi \rightarrow$ 3s transition. The CC2 and MRMP2 excitation energies are in excellent agreement with the MRCI values (MAD ≤ 0.03). TDHF and TDDFT/BH-LYP predict excitation energies for the Rydberg states that are correct on an absolute scale but slightly too high with respect to the $\pi \rightarrow \pi^*$ transition. With the BP86 and the B3-LYP functionals, the relative $\pi \rightarrow p_{y/z}$ energies are about 0.15 eV too low. Thus a functional-dependent, unbalanced description of Rydberg and valence excited states is observed, but unlike the situation with H_2S_2, the MAD values are comparatively small and of the same order of magnitude with all functionals. The DFT/MRCI method yields energies that are very similar to those calculated with TDDFT/BH-LYP.

With one exception ($\pi \rightarrow 3p_y$ transition with CC2), the signs of the rotatory strengths are correctly predicted. The most significant error is the overestimation of the rotatory strength of the $\pi \rightarrow \pi^*$ transition for all methods. The values for this transition obtained with the TDDFT methods decrease when HFXC increases. The worst result arises from the DFT/MRCI method, which overestimates the rotatory strengths by a factor of 2.5. The significant discrepancy between TDDFT/BH-LYP and DFT/MRCI is unexpected to some extent. The Cotton effect of the $\pi \rightarrow 3p_y$ transition is drastically overestimated if the BP86 functional is applied. This is due to an incorrect strong mixing of the $\pi \rightarrow \pi^*$ and $\pi \rightarrow 3p_y$ states, which in turn induces an electric moment in the latter that is too large and yields the much too intensive Cotton effect.

The rotatory strengths of the remaining transitions are not very dependent on the choice of a functional. Similar to the situation with H_2S_2, the BP86 functional causes by far the largest errors. As indicated by the MRD of <20%, the best agreement with the MRCI data is achieved with the MRMP2 method. According to our experience, however, this results mainly from the small size of the system and the fact that the MRMP2 transition moments are dominated by the reference wave function (which seems to be very good in this case). According to our experience, the transferability of the results for the model systems is rather limited, especially for the MRMP2 method.

3.1.3. 2,3-(*S*,*S*)-Dimethyloxirane (DMO) (1). Although DMO is a configurationally stable molecule for which accurate gas-phase CD spectra[46] are available, we consider it here to be a model compound for the large class of organic chromophores containing oxygen. The electronic spectrum of DMO is characterized by two overlapping Rydberg series. Valence excited states are not observed[47] below 9 eV. Our investigation is restricted to the first four Rydberg states originating from the nonbonding p-type lone pair on oxygen that is perpendicular to the three-membered ring. The partial π character of the highest σ MO in oxirane lying in the plane of the ring (comparable to cyclopropane) leads to an electronic structure that is similar to that of a carbonyl group, which will be investigated in more detail in section 3.2.1. The similarity between these chromophores is also reflected by the same local C_{2v} symmetry, which in DMO is reduced to C_2 by the two methyl substituents. Contrary to all other cases studied, a clear classification into inherently chiral and achiral-perturbed chromophores is not possible here because the substituents are quite close to the three-

TABLE 3: Excitation Energies (eV) and Rotatory Strengths (10^{-40} cgs units) for DMO (1)

state/classification	$\Delta E/R^r$	TDDFT BH-LYP[c]	TDDFT B3-LYP	TDDFT BP86	CC2	DFT/MRCI[c]	MRMP2[a]	MRCI	exptl[b]
1B	ΔE	6.97	6.97	6.97	6.97	6.97	6.97	6.97	6.97
n → 3s	R^r	18.6	13.0	11.0	17.4	23.2	11.5	12.1	9.5
2A	ΔE	7.28	7.33	7.40	7.27	7.31	7.26	7.31	7.35
n → $3p_1$	R^r	−19.3	−16.8	−12.0	−18.2	−11.8	−13.5	−16.5	−0.1
2B	ΔE	7.52	7.69	7.76	7.57	7.41	7.45	7.56	7.56
n → $3p_z$	R^r	10.5	8.3	7.2	10.2	11.2	6.9	10.5	6.2
3A	ΔE	7.49	7.40	7.32	7.59	7.51	7.59	7.63	
n → $3p_2$	R^r	3.1	6.1	0.8	4.4	1.8	2.1	5.9	
shift value (eV)[d]		−0.87	0.42	1.05	0.52	−0.52	0.17	0.06	
MAD[e]	ΔE	0.07	0.13	0.20	0.03	0.09	0.07		
MRD[f]	R^r	30%	8%	39%	21%	49%	30%		

[a] HF(N-1) orbitals; diffuse functions are on the center of charge of the cation. [b] Reference 46. [c] Calculation yields mixed $\sigma \rightarrow$ Ryd and n → Ryd series; see the text for details. [d] Shifts with respect to experimental excitation energy for the n → 3s transition; positive values indicate that the calculated excitation energies are too low. [e] Corresponds to the shifted excitation energies. The reference value was excluded. [f] Mean relative deviation.

membered ring and are also helically oriented. This becomes very obvious by visual inspection of the $3p_x$ and $3p_y$ Rydberg orbitals that are tilted by approximately 45° with respect to the axes of the C_{2v}-symmetric basis structure. This orbital mixing leads to a situation in which the so-called $3p_1$ orbital has almost no interaction with the remaining molecule but the $3p_2$ orbital points in the direction of the methyl groups. From previous ab initio work, it is known[47] that HF theory wrongly predicts the 1^2A^+ cation state (ionization out of a σ MO) to be lower in energy than the 1^2B^+ state (ionization out of the lone pair), which leads to an interchange of the two corresponding Rydberg series. Consequently, 1^2B^+ cation-type orbitals have been employed in the MRCI and MRMP2 treatments.

Results. Although our MRCI treatment including 30 correlated electrons (2.2×10^6 selected configurations at a threshold of $0.1E_h$) is at the limit of our capabilities and considerable size-consistency errors are to be expected, the excitation energies obtained with the MRCI method are in perfect agreement with the experimental data. Even though experimental data are available, we take the MRCI data as a reference because nonvertical effects seem to be of particular importance for the second (n → $3p_1$) band,[48] where a large discrepancy between all theoretical (−9.1 to −19.3) and experimental (−0.13) rotatory strengths is observed (Table 3).

The TDHF method suffers from the bad quality of the HF orbitals mentioned before. Within the first four transitions, three $\sigma \rightarrow$ Ryd type excitations are incorrectly predicted, and hence these results are not discussed further. As expected, similar problems arise from the TDDFT/BH-LYP approach. Although the ground-state calculation yields the correct orbital ordering in the Koopmans' sense, two $\sigma \rightarrow$ Ryd transitions (not shown) are observed in the energetic range of the n → 3s, p transitions. Furthermore, TDDFT/BH-LYP yields a mixed description for the latter, which is contradictory to that of the other methods (except DFT/MRCI). It is not surprising that the inadequate BH-LYP functional also causes difficulties with the DFT/MRCI method that is also based on this functional.

The excitation energies are shifted with respect to the MRCI result for the n → 3s transition. Opposed to the results discussed before, the CC2 treatment yields a systematic underestimation of the excitation energies by 0.52 eV. Since all of the considered transitions are of Rydberg type, this deviation is unexpected. The dependence of the systematic errors obtained for different functionals used in TDDFT is similar to that of H_2S_2 and ethylene. The relative excitation energies predicted by MRMP2 and CC2 are in satisfying agreement with the MRCI data (MAD 0.05 and 0.03 eV). Because of the imbalances between Rydberg and valence states, this is not true for the TDDFT method. Also, in accord with the results for H_2S_2, the MAD increases if HFXC decreases. The incorrect ordering of states 2A, 2B, and 3A is of particular interest. Considering the spatial dimensions of these transitions (2A, 2B: $\sim 50a_0^2$; 3A: $71.0a_0^2$), it is very probable that the error is due to the wrong asymptotic behavior of the functionals. As expected, the effect is weaker when using the BH-LYP functional, but the problem is still unresolved with 50% HF exchange. This example shows not only that the imbalanced description of valence and Rydberg states is problematic but also that the occurrence of Rydberg states with different spatial dimensions can cause significant errors.

All rotatory strengths are obtained with the correct sign. A relatively systematic underestimation of the absolute values is obtained with the MRMP2 method. The rotatory strengths obtained from the TDDFT calculations strongly depend on the fraction of exact exchange. A significant decrease in the values with HFXC is observed, which is, however, contradictory to the observations for H_2S_2. The substantial differences in the rotatory strengths of the n → $3p_1$ and n → $3p_2$ transitions between TDDFT/BH-LYP and DFT/MRCI indicate that both methods describe the electronic character of the excited states differently, although almost identical excitation energies are obtained. A comparable good overall performance for this system is obtained from the CC2 and MRMP2 treatments. Obviously, the CC2 method is able to compensate the bad HF description of the ground state. The TDDFT method suffers mainly from the wrong energetic ordering of the 3p Rydberg-type states. Out of the three functionals tested, B3-LYP (MRD of 8%) performs the best.

3.2. Real Systems. 3.2.1. (*R*)-Camphor (2) and (*R*)-Norcamphor (3). Because the carbonyl group is one of the most important functional groups in organic chemistry, appearing in many chiral natural substances, theoretical investigations of the CD of this chromophore is of major interest. The bicyclic ketones ((*R*)-camphor and (*R*)-norcamphor) investigated in this work have a locally C_{2v}-symmetric chromophore. The symmetry is perturbed by the bicyclic structure representing a chiral second sphere.[49] The n → π^* transition of these compounds has been extensively investigated since it appears in the near-UV region (~4 eV; 310 nm); therefore, the corresponding CD band is usually well separated and easy to assign. Much work has been

TABLE 4: Excitation Energies (eV) and Rotatory Strengths (10^{-40} cgs units) for (*R*)-Camphor (2)

state/classification	$\Delta E/R^r$	TDHF	TDDFT BH-LYP	TDDFT B3-LYP	TDDFT BP86	CC2[a]	DFT/MRCI	MRMP2[b]	exptl[c]
2A	ΔE	4.20	4.20	4.20	4.20	4.20	4.20	4.20	4.20
$n \rightarrow \pi^*$	R^r	1.5	3.2	5.4	8.1	5.6	3.4	5.9	4.5
3A	ΔE	7.45	6.59	5.66	5.21	6.07	6.94	6.26	6.24
$n \rightarrow 3s$	R^r	7.5	1.8	−2.8	−4.9	7.8	1.3	2.1	0.7
4A	ΔE	7.93	6.99	6.03	5.62	6.44	7.34	6.63	
$n \rightarrow 3p_1$	R^r	9.3	0.1	1.6	1.1	0.8	−0.8	0.4	
5A	ΔE	7.96	7.02	6.09	5.67	6.73	7.38	6.64	6.63[d]
$n \rightarrow 3p_2$	R^r	−4.8	2.8	−0.4	−0.2	8.8	2.8	−1.7	3.2[d]
6A	ΔE	8.093	7.09	6.16	5.80	6.81	7.52	6.70	
$n \rightarrow 3p_3$	R^r	0.9	3.0	4.1	2.7	−2.0	10.9	0.8	
shift value (eV)[e]		−0.78	−0.31	−0.03	0.17	−0.20	0.48	−0.18	

[a] Because of technical limitations, a reduced basis set with diffuse functions only at the carbonyl groups and the neighboring carbon atoms has been employed. [b] HF(N-1) orbitals; diffuse functions are on the center of charge of the cation. For exponents, see section 2. [c] References 50 and 51. [d] Average over all 3p states. [e] Shifts with respect to the experimental value for the $n \rightarrow \pi^*$ transition; positive values indicate that the calculated excitation energies are too low.

TABLE 5: Excitation Energies (eV) and Rotatory Strengths (10^{-40} cgs units) for (*R*)-Norcamphor (3)

state/classification	$\Delta E/R^r$	TDHF	TDDFT BH-LYP	TDDFT B3-LYP	TDDFT BP86	CC2[a]	DFT/MRCI	MRMP2[b]	exptl[c]
2A	ΔE	4.03	4.03	4.03	4.03	4.03	4.03	4.03	0.82
$n \rightarrow \pi^*$	R^r	0.4	1.1	1.0	0.7	1.6	1.6	−0.5	6.2
3A	ΔE	7.24	6.37	5.46	5.02	5.88	6.72	6.04	6.23
$n \rightarrow 3s$	R^r	−2.8	−3.2	−1.6	−0.1	−1.8	−3.1	−1.2	−3.0
4A	ΔE	7.80	7.02	6.02	5.59	6.30	7.31	6.52	
$n \rightarrow 3p_1$	R^r	7.0	15.5	6.7	3.6	3.4	13.5	1.9	
5A	ΔE	7.84	7.04	6.05	5.65	6.50	7.38	6.52	6.77[d]
$n \rightarrow 3p_2$	R^r	8.2	1.7	5.1	3.7	12.2	5.8	2.7	14.1[d]
6A	ΔE	7.97	7.10	6.09	5.72	6.64	7.47	6.58	
$n \rightarrow 3p_3$	R^r	7.6	−2.9	−2.1	−0.1	0.4	−4.2	2.0	
shift value (eV)[e]		−0.90	−0.47	−0.19	−0.01	−0.38	0.32	0.01	4.03

[a] Because of technical limitations, a reduced basis set with diffuse functions only at the carbonyl groups and the neighboring carbon atoms has been employed. [b] HF(N-1) orbitals; diffuse functions are on the center of charge of the cation. For exponents, see section 2. [c] References 50 and 51. [d] Average over all 3p states. [e] Shifts with respect to the experimental value for the $n \rightarrow \pi^*$ transition; positive values indicate that the calculated excitation energies are too low.

done to develop structure−chiroptic relationships for this transition, and the results have been summarized in the famous ketone octant rule.[4] The next-higher-lying transitions belong to the $n \rightarrow 3spd...$ Rydberg series, which starts at about 6 eV (207 nm).[50] The $n \rightarrow \pi^*$ transition is electric dipole-forbidden in the local C_{2v} symmetry of the chromophore, but the magnetic transition dipole moment is very strong. Thus, the situation is opposed to the $\pi \rightarrow \pi^*$ transition in monoenes (see below), which provide a large oscillator strength but a vanishing magnetic dipole moment. In both cases, weak Cotton effects whose sign is influenced only by the amount and direction of the perturbation of the local symmetry are observed. The small effects contributing to the CD of such compounds are not completely covered by semiempirical approaches such as the octant rule, which is, for example, reflected by its failure for the $n \rightarrow \pi^*$ transition in camphor.

A further impressive demonstration of the sensitivity of the camphor derivatives with respect to slight changes in the molecular structure is the opposite sign of the CD for the $n \rightarrow 3s$ transition in camphor and norcamphor. The different substitution patterns represent a change in the chiral third sphere, which usually does not affect the sign of a Cotton effect if the second sphere is also chiral.[49] This underlines that very weak effects play an important role here, which has prompted us to study both systems.

Results. For camphor and norcamphor, experimental gas-phase spectra are available.[50,51] In Tables 4 and 5, theoretical data for the first five transitions ($n \rightarrow \pi^*$ and the first four Rydberg transitions of the $n \rightarrow 3spd...$ series) are given. In the simulated spectra shown in Figures 2 and 3, 15 and 8 states were considered with TDDFT (BH-LYP and BP86) and CC2, respectively. The theoretical excitation energies are shifted with respect to the experimental value for the $n \rightarrow \pi^*$ transition. In contrast to those of DMO, the CC2 excitation energies are too high, which is rather unexpected considering the similar character of the Rydberg states. Similar results are found with MRMP2, though to a weaker extent. All in all, the relative excitation energies obtained with CC2 and MRMP2 are in good agreement with experiment, and no imbalanced treatment of Rydberg and valence states is observed.

The DFT/MRCI method is known for underestimating $n \rightarrow \pi^*$ excitation energies.[15] However, because of the lack of a better-suited "reference transition" and for the sake of consistency, these data are also shifted to match the experiment for the $n \rightarrow \pi^*$ state. This is the reason for the strong overestimation of the relative Rydberg excitation energies with this method. The TDDFT method suffers from an increasing underestimation of Rydberg excitation energies with decreasing HFXC that is already known from the model compounds. For both camphor derivatives, it leads to a "stretching" of the lower-energy

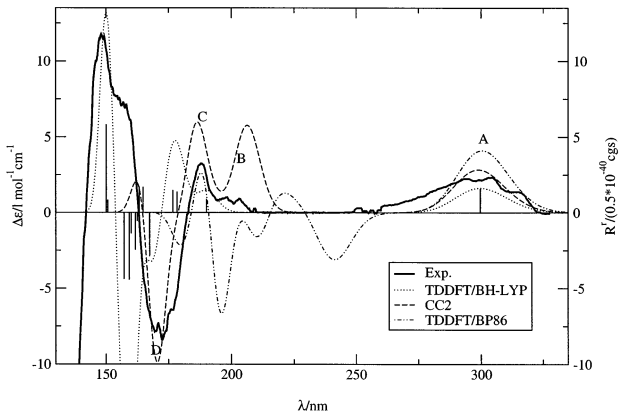

Figure 2. Comparison of theoretical and experimental CD spectra[50,51] of camphor (**2**). The bars indicate the excitation energies and rotatory strength of the transitions calculated with TDDFT/BH-LYP. The theoretical excitation energies have been shifted to match the A band. (See Table 4.)

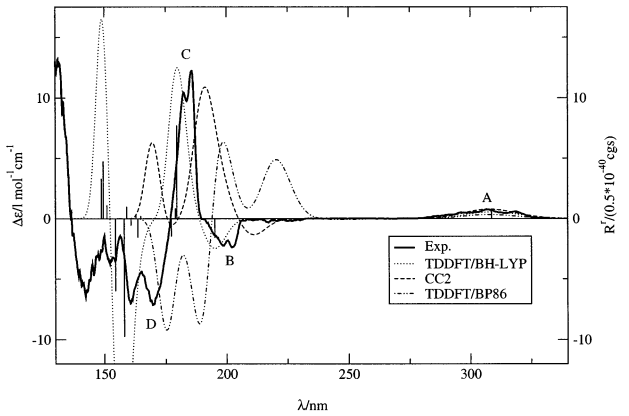

Figure 3. Comparison of theoretical and experimental CD spectra[50,51] of norcamphor (**3**). The bars indicate the excitation energies and rotatory strength of the transitions calculated with TDDFT/BH-LYP. The theoretical excitation energies have been shifted to match the A band. (See Table 5.)

Rydberg spectra. In other words, the spacings between the four 3sp states are too large with TDDFT/BP86 and decrease stepwise with the increase in HFXC. In contrast to what is found for the model compounds, the TDDFT/BH-LYP and DFT/MRCI results differ significantly. The $\sigma \rightarrow \pi^*$ transition that contributes to the D band in the camphor spectrum is essentially a charge-transfer transition. Because of the wrong description of this type of transition with TDDFT/BP86, the band splits up in the corresponding simulated spectra (Figure 2). The use of hybrid functionals can fix this problem to some extent. The TDDFT/BH-LYP spectrum is in almost perfect agreement with the experiment whereas with other functionals several inconsistencies in the signs of the rotatory strengths are obtained. With the B3-LYP and the BP86 functionals, TDDFT gives an n $\rightarrow$ 3s transition with the incorrect sign, yielding a significant mismatch of experiment and theory in the corresponding energetic range. (See Figure 2.) It is remarkable that the correct answer is obtained with B3-LYP if a reduced basis set is employed (SV(P), diffuse functions only at the chromophore atoms and at neighboring carbons). Furthermore, the description of the 3p states, which are individually not resolved in the experimental spectra, differs substantially. Although the sign of the "sum over 3p states" is reproduced by all methods except MRMP2, the signs of the individual transitions partially differ.

For norcamphor, the results are slightly better. The signs of the experimental bands are obtained correctly with all methods except MRMP2, which incorrectly predicts a negative sign for the Cotton effect of the important n $\rightarrow \pi^*$ transition. Taking into account the wrong sign of the C band in the camphor spectrum with this method, it is very probable that a satisfying description of these systems with MRMP2 in the framework of our standard procedure (one set of orbitals for all states) is not possible. The rotatory strength of the n $\rightarrow$ 3s transition is underestimated with the BP86 functional; therefore, this method is not able to reproduce the experimental B band (Figure 3). The best match of simulated and experimental spectra is achieved with the TDDFT/BH-LYP and the DFT/MRCI methods. (See Figures 2 and 3.)

The substantial deviations between the methods reflect the general problems with inherently achiral chromophores. The angles between the magnetic and electric transition dipole moments ($\angle(\vec{\mu}, \vec{m})$) determining the sign of the rotatory strengths (eq 2) are very often close to 90° in those types of systems. Therefore, slight changes in the wave function can cause considerable deviations in $\angle(\vec{\mu}, \vec{m})$ and thereby changes in the sign of the Cotton effect. For example, TDHF predicts $\angle(\vec{\mu}(L), \vec{m})$ to be 80° for the n $\rightarrow$ 3s transition (which corresponds to the correct sign) whereas TDDFT/BP86 gives 147°. Furthermore, even moderate changes in the basis set can cause changes in sign, as described above.

3.2.2. α-1,3-(*R*,*R*)-Pinene (4). The CD spectroscopic properties of α-pinene exhibit some similarity to those of the camphor derivatives: a locally achiral chromophore is embedded in a bicyclic system. Since the ethylene chromophore in α-pinene is 3-fold substituted, it is reasonable to assume local C_s symmetry of the chromophore rather than D_{2h} symmetry as in ethylene itself. In the C_s point group, all transitions of interest are electric and magnetic dipole-allowed, but the corresponding transition moments are perpendicular to each other. Because of the near degeneracy of the $\pi \rightarrow \pi^*$ state and the first members of the $\pi \rightarrow$ Rydberg series in α-pinene, extensive Rydberg−valence mixing of these states is observed. Consequently, there is no band in the CD spectra that exclusively corresponds to the $\pi \rightarrow \pi^*$ transition; therefore, the alkene octant rule[5] is not applicable. In contrast to the camphor derivatives, the perturbation of the local symmetry is not due to the bicyclic system, representing the second sphere,[49] but to the two methyl substituents and thus to the third sphere. Consequently, the perturbing effect is even weaker than in camphor. Additionally, the first Rydberg states gain intensity by mixing with the $\pi \rightarrow \pi^*$ transition. These considerations clearly indicate that the theoretical treatment of α-pinene is rather challanging and even more problematic than that of the camphor derivatives.

Results. The theoretical excitation energies (Table 6 and Figure 4) are shifted with respect to the $\pi \rightarrow$ 3s transition seen as the first transition in the experimental gas-phase spectrum.[52] The corresponding band splits because of vibronic coupling with the C=C stretching vibration;[52] therefore, an average value derived from the resulting two bands (5.66 eV; 219 nm) is taken as the vertical excitation energy.

The dependence of the shift values on the functionals and the overestimation of the energies by CC2 and MRMP2 are even more pronounced here than for the camphor derivatives. The $\pi \rightarrow \pi^*$/Rydberg mixing is described very differently by the various methods. In Table 6, transitions with considerable $\pi \rightarrow \pi^*$ contributions are indicated by the superscript d. In ref 52, the negative band at 6.2 eV (200 nm) in the experimental spectra is assigned to the $\pi \rightarrow \pi^*$ transition on the basis of the corresponding intense UV band. This assumption is confirmed by the TDHF calculation that predicts a significant $\pi \rightarrow \pi^*$

TABLE 6: Excitation Energies (eV) and Rotatory Strengths (10^{-4} cgs units) for α-Pinene (4)[a]

state/classification	$\Delta E/R^r$	TDHF	TDDFT BH-LYP	TDDFT B3-LYP	TDDFT BP86	CC2[b]	DFT/ MRCI	MRMP2[c]	exptl[d]
2A	ΔE	5.66	5.66	5.66	5.66	5.66	5.66	5.66	5.66
$\pi \rightarrow$ 3s	R^r	2.3	4.1	6.0	7.2	3.0	4.9	2.3	1.5
3A	ΔE	5.91[f]	6.08	6.05	6.04	5.87	6.07[f]	6.07	
	R^r	−20.7[f]	−34.6	−12.7	−11.1	−6.0	−46.1[f]	−2.7	
4A	ΔE	6.25	6.14	6.10	6.10	6.14[f,g]	6.14	6.12	6.10[h]
	R^r	2.4	8.1	0.8	−0.1	−21.8[f,g]	23.0	2.7	−6.1[h]
5A	ΔE	6.30	6.22	5.85	6.17	6.22[f,g]	6.24	6.18	
	R^r	−0.6	10.0	4.2	7.6	4.4[f,g]	9.4	−3.8	
6A	ΔE	6.51	6.27	6.07[f]	6.38[f]	6.34	6.30	6.64	
	R^r	6.7	8.6	5.4[f]	−6.3[f]	4.6	6.7	1.0	
shift value (eV)[e]		−0.77	−0.27	0.33	0.53	−0.46	−0.05	−0.63	

[a] Strong $\pi \rightarrow \pi^*$ mixing prevents a classification of the transitions. The vertical lines indicate the energetic range in comparison to the experimental spectra. [b] Because of technical limitations, a reduced basis set with diffuse functions only at the chromophore and at the neighboring carbon atoms has been employed. [c] HF(N-1) orbitals; diffuse functions are on the center of charge of the cation. For exponents, see section 2. [d] Reference 52. [e] Shifts with respect to the experimental excitation energy for the $\pi \rightarrow$ 3s transition; positive values indicate that the calculated excitation energies are too low. [f] Significant $\pi \rightarrow \pi^*$ contribution; see the text. [g] For technical reasons (section 2), assignment was deduced from oscillator strengths: $f(4A) = 0.0994$, $f(5A) = 0.0426$. [h] Values refer to band B in the experimental spectra.

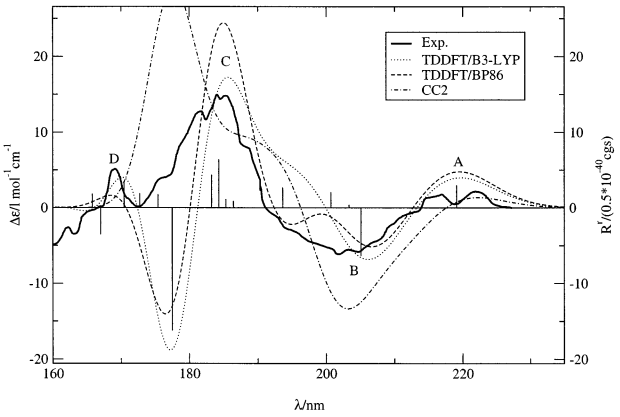

Figure 4. Comparison of theoretical and experimental[52] CD spectra of α-pinene (**4**). The bars indicate the excitation energies and rotatory strength of the transitions calculated with TDDFT/B3-LYP. The theoretical excitation energies have been shifted to match the A band. (See Table 6.)

contribution to the second transition. The TDDFT method yields very inconsistent results depending on which functional is used. With BH-LYP, 5 of the first 10 transitions exhibit $\pi \rightarrow \pi^*$ character to some extent, but none of them is dominated by this transition. If B3-LYP or BP86 functionals are employed, then a transition with almost pure $\pi \rightarrow \pi^*$ character is obtained as the fifth excited state. In contrast to TDDFT/BH-LYP, the DFT/MRCI method yields a 3A state that is mainly of $\pi \rightarrow \pi^*$ character comparable to that of TDHF. According to the oscillator strengths (see Table 6 annotation e), the CC2 method predicts two transitions (third and fourth) exhibiting some $\pi \rightarrow \pi^*$ character. Only the MRMP2 treatment completely lacks a $\pi \rightarrow \pi^*$ transition (within the first 10 excited states considered), which seems rather unexpected considering the good performance of this method for the ethylene model. These considerations show that the various methods predict different electronic character for all transitions except the $\pi \rightarrow$ 3s transition. Therefore, the data are not directly comparable, and the excitation energies are not discussed in detail, but the observations are qualitatively in line with those found for the camphor derivatives. The Rydberg excitation energies are underestimated by the pure BP86 functional, and an increasing HFXC causes an increase in the energies with respect to the $\pi \rightarrow \pi^*$ transition. Furthermore, the number of transitions that contribute to the experimental bands differs. (In Table 6, the transitions corresponding to an experimental band are separated by vertical lines).

The assignment problems also prevent a detailed comparison of the rotatory strengths. Nevertheless, all methods agree on the signs of the experimental A and B bands, although the contributions to B varies as described above. The TDDFT/BP86 calculation predicts an incorrect splitting of the B band, leading to a mismatch of the simulated and experimental spectra between 190 and 210 nm (Figure 4). The rotatory strengths obtained with the MRMP2 method are significantly too low, which is probably due to the lack of $\pi \rightarrow \pi^*$ contributions. All methods fail in the description of the area above the C band. All DFT-based methods predict a strongly negative band around ∼7.0 eV (177 nm), which has no counterpart in the experimental spectrum.

Obviously, none of the considered methods correctly describes the important Rydberg−valence mixing occurring in α-pinene. Therefore, despite the relatively good visual match of theory and experiment in the area of the first three bands, the theoretical results should be considered carefully. However, the simultaneous application of different methods is, in our opinion, an appropriate tool for detecting problematic systems.

3.2.3. 2,3-(*S,S*)-Dithiadecaline (7). The properties of the disulfide chromophore have been described in section 3.1.1. The identical dihedral angles ϕ^{RSSR} of the model compound and 2,3-(*S,S*)-dithiadecaline (DTD) and the fact that they have the same symmetry (C_2) should provide transferability of the results to a certain extent. In particular, the properties of transitions among orbitals that are almost localized at the chromophore, namely, the first two transitions, are expected to be very similar to those of the model compound. The higher valence states in H_2S_2 where σ(SH)* orbitals are involved are obviously less similar than the corresponding σ(SC)* states in DTD.

The experimental spectrum in ref 53 has been measured in hexane. Because all excited states in DTD show Rydberg contributions, solvent effects may be of some importance, and this has to be kept in mind when discussing the theoretical predictions. The investigations of DTD have been performed

TABLE 7: Excitation Energies (eV) and Rotatory Strengths (in 10^{-40} cgs units) for 2,3-(*S*,*S*)-Dithiadecaline (7)

state/classification	$\Delta E/R^r$	TDHF	TDDFT BH-LYP	TDDFT B3-LYP	TDDFT BP86	CC2	DFT/ MRCI	MRMP2[a]	exptl[b]
1B	ΔE	4.25	4.25	4.25	4.25	4.25	4.25	4.25	4.25
$n_a \rightarrow \sigma(SS)^*$	R^r	−16.2	−14.5	−14.4	−12.9	−18.8	−18.1	−32.2	−14.3
2A	ΔE	5.38	5.30	5.19	5.07	5.24	5.15	5.45	5.10
$n_b \rightarrow \sigma(SS)^*$	R^r	12.3	12.5	10.8	4.5	11.0	10.7	15.1	11.4
3A	ΔE	6.21[d]	5.88	5.57	5.40	5.61	5.59	5.99	
$n_a \rightarrow \sigma(SC)_1^*$	R^r	−11.5[d]	−0.1	6.8	13.1	−1.2	7.8	−12.6	
4A	ΔE	6.67[d]	6.35	5.95	5.85	6.07	6.28	6.18	
$n_a \rightarrow 3s$	R^r	−33.3[d]	−39.3	−39.8	−32.9	−41.0	−54.9	−29.5	
2B	ΔE	6.55[d]	6.33	5.91	5.77	6.12	6.16	6.59	5.99[e]
$n_a \rightarrow 3p_1$	R^r	48.7[d]	10.6	−21.8	−32.4	−10.2	3.5	8.4	−68.6[e]
3B	ΔE	7.06[d]	6.67	6.10	5.92	6.43	6.64	6.87[f]	
$n_a \rightarrow 3p_2$	R^r	29.0[d]	−32.4	−19.1	−16.3	−32.8	30.7	−42.0[f]	
4B	ΔE	7.15[d]	6.76	6.45	6.25	6.51	6.54[d]	6.89	
$n_b \rightarrow \sigma(SC)_1^*$	R^r	−90.3[d]	−16.4	21.5	6.2	−5.6	−88.1[d]	11.1	
5A	ΔE	7.69[d]	7.22	6.45	6.13	7.01	7.11	*g*	
$n_a \rightarrow 3p_z$	R^r	−4.0[d]	2.4	3.4	−4.7	1.6	3.9	*g*	
shift value (eV)[c]		−0.29	0.12	0.39	0.55	0.10	0.42	0.47	

[a] HF(N-1) orbitals; see text. [b] Reference 53. [c] Shifts with respect to the experimental excitation energy for the $n_a \rightarrow \sigma(SS)^*$ transition; positive values indicate that the calculated excitation energies are too low. [d] Classification is difficult because of strong state mixing. [e] Values refer to band C in the experimental spectrum. [f] $n_a \rightarrow \sigma(SC)_2^*$ state. [g] Value not calculated.

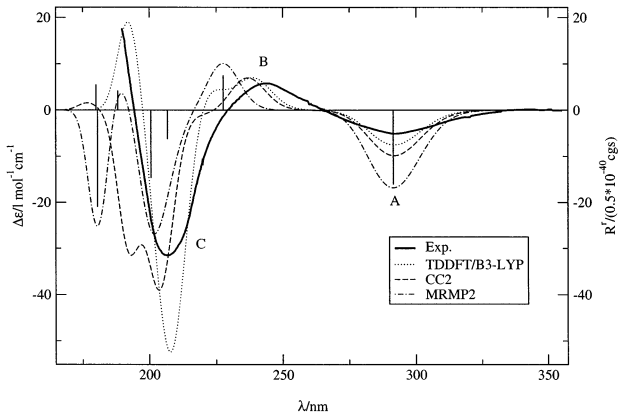

Figure 5. Comparison of theoretical and experimental[53] CD spectra of 2,3-(*S*,*S*)-dithiadecaline (**7**). The bars indicate the excitation energies and rotatory strength as obtained with MRMP2. The theoretical excitation energies have been shifted to match the A band. (See Table 7.)

with the aug-TZVPP basis set at the sulfur atoms as well as at the neighboring carbon atoms and the TZVP basis for the remaining atoms, as suggested by the model calculations on H_2S_2. In the MRMP2 treatment, the aug-TZVPP basis was employed only for the sulfur atoms.

Results. The theoretical excitation energies (Table 7 and Figure 5) are shifted with respect to the $n_a \rightarrow \sigma(SS)^*$ transition observed experimentally around 290 nm. As already mentioned in section 3.1.1, the classification of the transitions in a simple MO picture reaches its limits in the case of the disulfide chromophore, and this holds even to a stronger extent for DTD. As discussed before, for DTD an imbalanced description of states with different spatial dimensions is also observed in the TDDFT treatments. It is remarkable that in contrast to H_2S_2 the best results are obtained with the B3-LYP functional. The interchange of states 4B (more valence character) and 5A (more Rydberg character) with TDDFT/BP86 seems again to be induced by the wrong asymptotic behavior of the functional. TDDFT/BH-LYP and DFT/MRCI predict very similar relative excitation energies. The TDHF method is obviously not suitable for DTD. Except for the first two transitions, the results are not reasonable. In contrast to CC2 and MRMP2, TDDFT (with all functionals) incorrectly predicts the $n_a \rightarrow 3p_1$ transition to be energetically lower than the $n_a \rightarrow 3s$ transition. This is a consequence of the asymptotically wrong exchange correlation potential of the DFT functionals, which because of their different spatial dimensions has a greater effect on p states than on s states.

Although the angles $\angle(\vec{\mu}, \vec{m})$ in DTD are in general far away from 90°, only for three out of the eight investigated transitions do all methods agree on the signs of the Cotton effects. The rotatory strengths of the first two transitions $n_a \rightarrow \sigma(SS)^*$ and $n_b \rightarrow \sigma(SS)^*$ are all of acceptable accuracy (except for the value obtained with MRMP2, which is about twice as large.) The Cotton effect of the $n_a \rightarrow 3s$ transition that represents the main contribution to the C band is also obtained with the correct sign by all methods. The two transitions leading to $\sigma(SC)_1^*$-type excited states are theoretically the most demanding. Although the electric and magnetic transition dipole moments are parallel (as determined by symmetry), even the sign of the Cotton effect seems to be unpredictable. The TDDFT/BH-LYP, CC2, and MRMP2 calculations yield a negative sign whereas the opposite result is obtained with the other methods. Within the TDDFT calculations, substantial changes occur if different functionals are applied. The $n_a \rightarrow \sigma(SC)^*$ transition, for example, is predicted to influence the shape of the B band if B3-LYP or BP86 is used, but with BH-LYP, the sign is opposite and the contribution to the band is very small.

The shape of the experimental spectra is reproduced by all methods to a satisfying extent, although (as indicated by the vertical lines in Table 7) the number of contributing transitions, in particular, the number contributing to the C band, and the intensities vary substantially. According to the MRMP2 results,

TABLE 8: Excitation Energies (eV) and Rotatory Strengths (10^{-4} cgs units) for 4,5-Dimethylphenanthrene (8)

state/classification	$\Delta E/R^r$	TDHF	TDDFT BH-LYP	TDDFT B3-LYP	TDDFT BP86	CC2	DFT/ MRCI	MRMP2[a]	exptl[b]
2A	ΔE	4.26	3.94	3.89	3.89	3.44	3.44	3.16	3.6[d]
L_b	R^r	0.9	0.9	0.9	1.0	1.0	0.9	0.3	
1B	ΔE	4.05	4.05	4.05	4.05	4.05	4.05	4.05	4.05
L_a	R^r	−11.1	−20.5	−21.3	−19.7	−33.4	−35.7	−24.8	−19.5
3A	ΔE	5.66	4.89	4.61	4.47	4.58	4.64	4.54	4.58
B_b	R^r	193.0	161.1	109.1	77.3	136.8	165.5	153.1	67.8
2B	ΔE	5.33	5.04	4.98	4.90	4.90	4.93	4.77	5.00
B_a	R^r	−148.6	−103.7	−73.0	−39.2	−46.4	−84.6	−97.2	−24.4
shift value (eV)[c]		−0.40	−0.29	0.04	0.36	−0.55	−0.27	−0.41	

[a] HF orbitals. [b] Reference 57. [c] Shifts with respect to the experimental excitation energy for L_a; positive values indicate that the calculated values are too low. [d] No experimental data available. The given value corresponds to phenanthrene[58] corrected by theoretical data; see the text.

the C band is due to the $n_a \rightarrow \sigma(SC)_1^*$ and $n_a \rightarrow 3s$ transitions whereas TDDFT predicts at least three contributions that are all of Rydberg type. Taking into account that the experimental spectrum was recorded in hexane the C band very probably includes a valence transition that is in agreement with the results of the MRMP2 method.

Although the overall agreement of the theoretical and experimental spectra for DTD is rather good, the sensitivity of the results for individual states is disappointing, especially in comparison to the H_2S_2 model where this was not the case. This example shows clearly that calibration on model systems may not give any valuable insight into the properties of a real system.

3.2.4. (*M*)-4,5-Dimethylphenanthrene (8). The 4,5-dimethylphenanthrene (DMP) molecule can be considered to be the smallest member of the helicene family. Because the entire molecule forms an extensive, inherently chiral chromophore in these systems, the helicenes exhibit remarkably large optical rotation[54] and very intense Cotton effects in the near-UV region.[22] These properties have been of considerable importance to the understanding of chiroptical phenomena in general and have inspired the development of several chiroptical rules. (See the summary in ref 55.)

The symmetry of the helicenes is C_2. Thus, the relative orientation of the transition moments is determined by the same restrictions as those already discussed for the disulfide chromophore. DMP is a 14 π-electron system providing a relatively large density of one-electron states close to the HOMO energy. This is one of the reasons for the relatively strong configuration mixing of the states considered that are of pure valence $\pi \rightarrow \pi^*$ character. Although about 12 transitions are obtained up to 6.2 eV (200 nm), only a few of them significantly contribute to the shape of the CD spectra. In the near-UV region (up to ~5 eV, 248 nm), the dominating transitions are essentially those corresponding to free-electron states L_a, L_b, B_a, and B_b (Platt nomenclature; see ref 56). These states will be the main focus of the following investigation. For the higher excited states, a discussion is difficult because of pronounced mixing and the lack of an appropriate description of double and higher excitations with TDDFT and CC2. (See the following discussion.)

The experimental spectrum[57] was recorded in a mixture of ethanol and *n*-hexane. Since the ground and excited states exhibit dipole moments of comparable (small) magnitude and since no Rydberg transitions are of interest, this should not cause any significant deviations from the gas-phase spectra.

Results. The lowest electronic transition in DMP is into the L_b state, which arises from the two almost degenerate configurations HOMO → LUMO+1 and HOMO-1 → LUMO with a slightly larger weight of the former. The B_b state exhibits similar contributions, but here the HOMO-1 → LUMO contribution is larger. The L_a state is dominated by the HOMO → LUMO transition (~ 80%) and additionally contains some HOMO-1 → LUMO+1 contribution. By analogy to the L_b/B_b relation, there is a B_a state that is a "counterpart" to the L_a state, which is mainly formed by the HOMO-1 → LUMO+1 excitation.

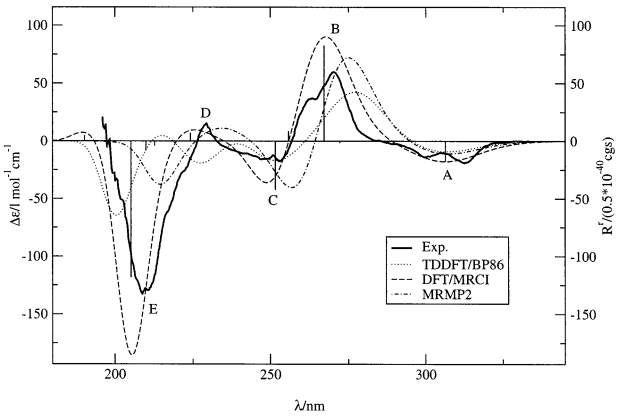

Figure 6. Comparison of theoretical and experimental CD spectra[57] of dimethylphenanthrene (**8**). The bars indicate the excitation energies and rotatory strength as obtained by DFT/MRCI. The theoretical excitation energies have been shifted to match the A band. (See Table 8.)

Besides these states, several additional transitions are observed above 5 eV (248 nm). The corresponding states exhibit very different electronic characteristics depending on the method applied. One important reason for this observation is the inability of TDDFT/TDHF and CC2 to describe double and higher excitations. That necessarily leads to inconsistencies between these methods and multireference approaches such as MRMP2 and DFT/MRCI. Even the number of predicted excited states partially differs. Therefore, a reasonable comparison of the states above 5 eV (248 nm) for all methods is not possible; consequently, Table 8 is restricted to the free-electron states described above. For the simulation of the CD spectra in Figure 6, however, 14 (DFT/MRCI and TDDFT/BH-LYP) and 11 (MRMP2) excited states have been included. The results (Table 8) are shifted with respect to the L_b transition (4.05 eV is taken as the excitation energy; the value has been obtained as an average over the vibronic structure observed).

The interchange of the B_b and B_a states as well as the L_b and L_a state calculated with TDHF indicates the inability of this method to describe the DMP system. This failure reflects the different properties of the L_a and B_a states, which are predomi-

nantly influenced by dynamic correlation, with respect to the L_b and B_b states, where static correlation is more important. Therefore, the errors caused by missing electron correlation (static and dynamic) in TDHF are not expected to be canceled. However, the TDDFT method (at least implicitly) accounts for both dynamic and static electron correlation, and a much better description of this problem is observed. With all applied functionals, TDDFT yields consistent energies for the L_a, L_b, and B_a states. Only the excitation energies of the B_b state decrease considerably with HFXC. A probable explanation for this finding is the higher importance of doubly excited configurations in the B_b state that TDDFT cannot account for. (According to the DFT/MRCI results, the most important double excitation has an amplitude of about 0.1.)

Since there is no available experimental value for the excitation energy of the L_b state, it is difficult to judge the quality of the TDDFT values. Taking the experimental value for the L_b state in phenanthrene (3.8 eV; ref 58) and assuming a red shift of 0.2 eV (as coincidently predicted by DFT/MRCI and CC2) due to the twisting and the methyl groups, the TDDFT methods overestimate the excitation energy. This is also confirmed by the significantly lower energies predicted by DFT/MRCI and CC2. MRMP2 underestimates the excitation energy. The rotatory strengths of the four L/B transitions are obtained without errors in sign but with partially significantly different absolute values. Within the TDDFT treatments, the Cotton effects of the B_b and the B_a transition decrease with decreasing HFXC from 161.1 (BH-LYP) to 77.3 (BP86) and from −148.6 (BH-LYP) to −39.2 (BP86). The DFT/MRCI and MRMP2 approaches yield values comparable to those of TDDFT/BH-LYP.

A favorable description of all experimental CD bands (see Figure 6) is achieved only by the TDDFT/BH-LYP, DFT/MRCI, and MRMP2 methods. CC2 gives slightly worse results since the intensity of the D band is too low. Despite the overestimated intensities of the B and C bands, the best agreement is obtained with the DFT/MRCI method. In cases such as DMP where double excitations are important, this method is clearly superior to TDDFT. As mentioned in the beginning, for the higher transitions that form the D and E bands, very nonuniform results are obtained with TDDFT depending on which functional is used. This reflects the increasing importance of higher excitations not included in TDDFT. The BP86 functional, for example, yields the wrong sign in the area of the D band (see Figure 6) where only the TDDFT/BH-LYP functional yields a good visual match of the spectra. However, the electronic character of the corresponding excited state differs from what is predicted by MRMP2 and DFT/MRCI; therefore, the good agreement with experiment is probably fortuitous. DMP is close to the limit of what is today computationally feasible with MRMP2 and CC2 methods. Therefore, the spectra simulated with the MRMP2 data cannot considered to be reliable in the range of the E band since not enough excited states could be calculated with sufficient accuracy.

3.2.5. (*S*)-Cyclohepta[1,2-b:1,7-b′]bis[1,4]-benzoxazine (9). At first glance, (*S*)-cyclohepta[1,2-b:1,7-b′]bis[1,4]-benzoxazine (CBB) appears very similar to the helicenes. It provides a helically distorted, C_2-symmetric π-electron system that extends over the whole molecule. Furthermore, optical rotatory power of a comparable order of magnitude is observed ($[\alpha]_D$ = −4700°; ref 59). Despite these similarities, the electronic properties differ considerably. The first six excited states that are considered in this work are all dominated by one singly excited configuration, in contrast to the strong mixing found for DMP. It is interesting that almost all of these transitions are of the HOMO-n → LUMO (n = 1...6) type.

A second point is the localization of some of the π orbitals. Whereas in helicenes a rather uniform electron distribution of all $\pi-$ orbitals leads to transitions with little charge separation, the opposite holds for CBB. The LUMO (39b) in CBB is almost localized at the seven-membered ring whereas the occupied $\pi-$ orbitals have larger amplitudes at the benzene rings. Orbitals 37b and 39a, for example, can be considered to be positive and negative linear combinations, respectively, of benzene-type e_1g orbitals of the two phenyl fragments of CBB. Consequently, the dipole moments of all of the excited states are larger than that of the ground state, and the 37b → 39b and 39a → 39b excitations can be considered to be typical charge-transfer (CT) transitions. Since the experimental CD spectrum was recorded in methanol, a stronger stabilization of the more polar excited states relative to that of the ground state is expected. Hence, the comparability between the theoretical and experimental data is somewhat limited compared to that of the other systems discussed so far.

Results. All excitation energies have been shifted with respect to the HOMO → LUMO transition observed experimentally at 3.1 eV (400 nm). In contrast to the previous systems, we want to open the discussion with some results of the MRMP2 calculation, which gives us a better understanding of the errors from the TDDFT treatments. According to the MRMP2 results, the spectrum is dominated by three very intense transitions corresponding to the 1B, 2A, and 4A states. The 1B (HOMO → LUMO) and 4A states exhibit moderate dipole moments of 0.45 and 1.81 D (Table 9), respectively, whereas for the 2A state a dipole moment of 4.16 D is predicted. Strong charge separation is also observed for the 1A → 3A (5.71 D) and 1A → 2B transitions (5.46 D). The CT character is furthermore responsible for the small rotatory strengths of these transitions, which do not affect the simulated spectra. Orbitals 38a and 36b obtained as HOMO-4 and HOMO-5 with HF and DFT/BH-LYP are interchanged with the B3-LYP and BP86 functionals. The classification in Table 9 is based on the DFT/BH-LYP ordering.

The relative excitation energies obtained with TDDFT generally decrease with decreasing HFXC. Because of their significant dipole moments, the largest effect is observed for the 3A and 2B states. The energies decrease from 4.09 and 4.22 eV to 3.35 and 3.44, respectively when going from BH-LYP to BP86. Similar behavior was observed for the 2A state, which plays an important role because of its strong Cotton effect. Corresponding to the 4A state obtained with MRMP2 and DFT/MRCI, the TDHF and TDDFT (BH-LYP and B3-LYP) response methods predict two states with rather similar but differently weighted contributions. The higher-lying transitions predicted by TDDFT/BP86 have no similarity to the other methods. The DFT/MRCI energies are in general about 0.5 eV below their TDDFT/BH-LYP counterparts and are very similar to the CC2 results.

The two methods based on HF orbitals (TDHF and MRMP2) predict different signs for the Cotton effects of the 1A → 3A, 2B, and 3B transitions than the DFT (including DFT/MRCI) methods. Furthermore, in accord with the results for the B_a and B_b states in DMP, the rotatory strengths of the three dominating transitions decrease with decreasing HFXC. The value for the HOMO-1 → LUMO transition, for example, decreases from 687.4 (TDHF) to 56.5 (TDDFT/BP86). In particular, deviations

TABLE 9: Excitation Energies (eV) and Rotatory Strengths (10^{-40} cgs units) for (*S*)-Cyclohepta[1,2-b:1,7-b′]bis[1,4]-benzoxazine (9)

state/classification[a]	$\Delta E/R^r$	TDHF[b]	TDDFT BH-LYP	TDDFT B3-LYP	TDDFT BP86	CC2[c]	DFT/ MRCI	MRMP2[d]	exptl[e]
1B	ΔE	3.11	3.11	3.11	3.11	3.11	3.11	3.11	3.11
HOMO → LUMO	R^r	−664.9	−592.7	−517.4	−451.1	−545.4	−648.5	−594.6	−217.1
$\langle\hat{r}\rangle^h$								1.84	
2A	ΔE	3.99	3.71	3.39	3.08	3.24	3.27	4.04	
HOMO−1 → LUMO	R^r	687.5	295.5	120.8	56.5	162.9	195.9	153.2	
$\langle\hat{r}\rangle^h$								4.16	
3A	ΔE	4.95	4.09	3.64	3.35	3.57	3.66	3.99	
HOMO−2 → LUMO	R^r	−71.9	8.3	3.5	14.3	52.0	6.0	−0.9[i]	
$\langle\hat{r}\rangle^h$								5.71	
2B	ΔE	4.88	4.22	3.79	3.44	3.75	3.77[j]	4.01	4.34
HOMO−3 → LUMO	R^r	−52.9	32.0	11.4	4.5	30.3	35.2[j]	−0.5	268.7
$\langle\hat{r}\rangle^h$								5.46	
3B	ΔE	5.24	4.49[k]	4.26[j]	3.92	4.15	4.08[k]	4.55	
HOMO−4 → LUMO	R^r	18.3	−25.5[k]	−2.9[j]	−29.4	−36.1	−7.4[k]	19.4	
$\langle\hat{r}\rangle^h$								1.50	
4A[l]	ΔE	4.57	4.50	4.08	3.78	4.18	4.00	4.01	
HOMO → LUMO+1/	R^r	45.0	325.8	56.9	5.5	93.3	185.5	339.2	
HOMO-5[g] → LUMO								0.45	
shift value (eV)[f]		−0.55	−0.09	0.32	0.62	−0.28	−0.04	−0.66	

[a] All transitions occur between π orbitals; exceptions are indicated. [b] Unlike all other methods, TDHF predicts an additional $\sigma \rightarrow \pi$ transition at ΔE(rel) = 5.47 eV. [c] Tentative assignments based on the transition properties and excitation energies. [d] HF orbitals. [e] Reference 59. [f] Shifts with respect to the experimental excitation energy for the HOMO → LUMO transition; positive values indicate that the calculated excitation energies are too low. [g] σ orbital; see the text. [h] Dipole moment in debye from the MRMP2 calculation; the ground-state value is 0.23 D. [i] Dipole velocity form for R has a different sign. [j] Significant contribution from HOMO−6(σ-MO) → LUMO. [k] Mixed state: HOMO−3,4,6(σ-MO) → LUMO. [l] Contributions strongly differ; see the text.

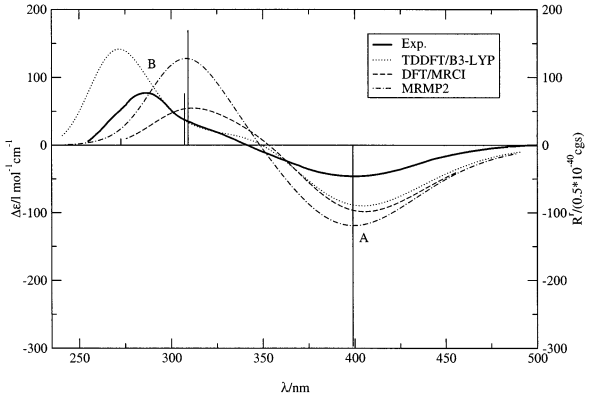

Figure 7. Comparison of theoretical and experimental CD spectra[59] of CBB (**9**). The bars indicate the excitation energies and rotatory strength as obtained with MRMP2. In contrast to previous simulations, a bandwidth of σ = 0.38 eV was used. The theoretical excitation energies have been shifted to match the A band. (See Table 9.)

between TDDFT/BH-LYP and DFT/MRCI are observed for transitions with important double-excitation contributions (e.g., 2A, 4A). Another important point is the good agreement between dipole velocity and the dipole length form of the rotatory strengths obtained with MRMP2, which is in contrast to that of the other systems treated in this work except DMP. It seems to be a general feature of inherently delocalized π systems.

The shapes of the simulated spectra are very similar, and even the TDDFT/BP86 and TDHF spectra are in reasonable agreement with experiment. One reason for this good match is the small CD intensities of the problematic charge-transfer transitions (2B, 3A). According to TDDFT/BH-LYP, they appear in the middle of the B band whereas BP86 places them in the range of the A band. The differences between the simulated spectra are mainly due to the HOMO-1 → LUMO transition (Figure 7). The corresponding Cotton effect is predicted by TDDFT/BH-LYP and MRMP2 to be very strong, and the transition contributes to the B band whereas it has a negligible effect on the spectra simulated with TDDFT(B3-LYP or BP86) and CC2 because of cancellation effects. With these functionals, the rotatory strengths of the transitions, which according to MRMP2 form the B band, are comparably weak, but because of higher-lying transitions with strong Cotton effects, the simulated spectra are not affected. One possible reason for this finding is the inability of the single-reference methods to describe the higher-lying excitations in CBB. This partially leads to the appearance of additional "unphysical" states (ghost states), which is more pronounced in CT systems.

3.2.6. (2*R*)-η^4-[3-(Tertbutyldimethylsiloxy-methyl)-penta-2,4-dienal]-tricarbonyl-iron(0) (10). The description of transition-metal compounds in general remains a challenging goal in quantum chemistry. The importance of static correlation effects arising from the near degeneracy within the metal d shells causes difficulties in single-reference treatments. Moreover, the bad quality of the Hartree−Fock orbitals for transition-metal compounds complicates the application of approaches lacking an appropriate description of orbital relaxation effects.

The transition-metal compound investigated in this work (**10**) is a typical example of a planar chiral molecule. Its classification in the sense of the local chirality of the chromophore is not straightforward. The molecule contains two achiral chromophores (pent-2,4-dienal and the $Fe(CO)_3$ fragment) that, attached to each other, form the chiral system. Nevertheless, the small $\Delta\epsilon$ values observed for **10**[60] indicate a similarity to the molecules with inherently achiral chromophores investigated in sections 3.2.1 and 3.2.2.

The spectroscopic activity of **10** in the near-UV region mainly originates from metal 3d → π^* transitions. As a result of the similar energies of the corresponding excited states, extensive mixing that also includes n → π^* transitions is observed.

Results. The OTBDMS group in **10** that has no excited states in the energetic range of interest was replaced by a hydrogen atom. A comparison of TDDFT/BP86 data with and without the OTBDMS group as well as the almost perfect match between

the spectra of **10** and that of a derivative with a hydroxy instead of an OTBDMS group (ref 61) confirms the validity of this procedure. Contrary to all other systems studied so far, **10** has flexible degrees of internal motion that have to be considered. Two conformers of the aldehyde ligand, namely, the *s*-cis and *s*-trans forms, have been investigated. Several methods were applied to determine their relative stabilities (ΔE). The dipole moment of the *s*-trans form was found to be significantly greater than that of the *s*-trans conformer (4.48 compared to 3.59 D; BP86/TZVPP) such that the solvent is expected to have a considerable influence on ΔE. The effect has been taken into account by employing the continuum solvation model COSMO.[62] Assuming a permittivity of 32.6 (the spectrum was recorded in methanol), the RIDFT/BP86 method favors the *s*-trans form by 1.24 kcal/mol (compared to a relative stability of −0.14 kcal/mol in the gas phase). MP2 and MRMP2 predict the *s*-trans conformer to be more stable (by 2.7 and 2.3 kcal/mol, respectively) even in the gas phase. On the basis of these results, we consider the *s*-trans conformer to be predominant. Therefore, mainly the results obtained for this form are discussed, but it would also be interesting if theoretical CD spectroscopy were able to resolve this stereochemical problem. The rotation of the $Fe(CO)_3$ moiety has been considered in a similar complex[51] but has been found not to influence calculated CD spectra significantly.

In accordance with the results for cases with strongly mixed states presented heretofore, the electronic nature of the excited states in **10** is described very differently depending on which method is applied. Furthermore, the energetic ordering and character of the MOs differ substantially between Hartree−Fock-based and DFT approaches as well as among different DFT functionals. Therefore, a reasonable direct comparison of the results with the help of an MO-based classification of the excited states is not possible. Hence, for the discussion of the **10** results, a different procedure is chosen: First, the electronic character and the excitation energy of the n → π* transition are considered in detail for the example of the *s*-trans conformer. (Very similar results are obtained for the *s*-cis form.) Second, experimental and theoretical data are qualitatively compared on the basis of the simulated theoretical spectra (Figure 7). They have been shifted with respect to the experimental B band, and the following shift values were applied (first and second values refer to the *s*-cis and *s*-trans conformers, respectively): 0.30/0.31 eV (TDDFT/BH-LYP); −0.09/−0.02 eV (TDDFT/B3-LYP); −0.25/−0.21 eV (TDDFT/BP86). Furthermore, because of the complexity of the electronic structure of **10**, reasonable results could not be obtained with CC2 and MRMP2 methods, and thus mainly the DF-based approaches (15 excited states have been calculated) will be discussed.

The carbonyl group in the aldehyde ligand is part of a conjugated π system that lowers the n → π* excitation energy compared to that of simple carbonyl groups, where it occurs around 4 eV. In fact, the first transition (2.90 eV, 428 nm) obtained with the TDDFT/BP86 treatment has almost pure n → π* character, and the sign of the rotatory strength matches that of the first experimental band (Figure 8). According to all other methods, the n → π_4^* transition is strongly mixed (Table 10) and does not correspond to this band. TDDFT/B3-LYP predicts a comparatively weak Cotton effect for the n → π_4^* transition (obtained as the 4A state with this method) such that the shape of the simulated spectrum is not influenced. TDDFT/BH-LYP and DFT/MRCI yield a mixing of the n → π_4^* and π_3 → π_4^* states. The resulting transition has comparatively great rotatory strength and appears at the eighth and sixth positions, respectively. In the case of TDDFT/BH-LYP, this leads to a positive band at ∼190 nm that is not seen experimentally.

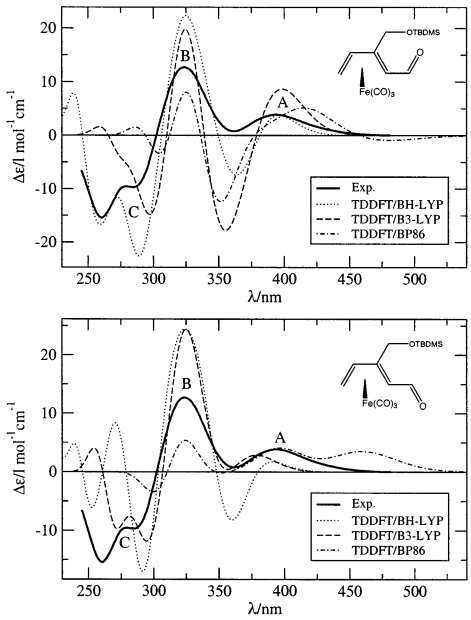

Figure 8. Comparison of theoretical and experimental CD spectra[60] of **10**. The theoretical excitation energies have been shifted to match the B band. The OTBDMS group has been substituted by a hydrogen atom. (See the text.)

TABLE 10: Description of the n → π* State of the *s*-trans Conformer of 10 by Different Methods

method	state	ΔE	R^r	contributions
TDDFT/BP86	2A	2.90	9.7	∼100% n → π_4^*
TDDFT/B3-LYP	4A	3.64	4.8	51% n → π_4^*
TDDFT/BH-LYP	9A	4.28	23.5	40% n → π_4^*; 19% π_3 → π_4^*
DFT/MRCI	7A	4.33	24.5	20% n → π_4^*; 20% π_3 → π_4^*

The number of transitions contributing to the first three bands is different for all of the methods. By far the best agreement with the experimental spectrum is achieved with TDDFT/B3-LYP. TDDFT/BH-LYP predicts an incorrect negative band at ∼360 nm and completely fails in the description of the area above ∼300 nm. DFT/MRCI (not shown in Figure 8) performs slightly better, but the agreement is also not satisfying. The spectra obtained on the basis of the CC2, MRMP2, and TDDFT/BP86 data provide almost no similarity with the experiment such that a presentation of the results is omitted for CC2 and MRMP2. (BP86 is included in Figure 8 for the sake of comparability within TDDFT.)

The two conformers of **10** (*s*-cis and *s*-trans) are expected to be distinguishable on the basis of their CD spectra. A consideration on the basis of the octant role, for instance, leads to opposite signs for the n → π_4^* transition. Indeed, the theoretical (TDDFT) spectra do not differ significantly for both conformers (Figure 8). The calculations carried out with the BP86 and B3-LYP functionals yield slightly better agreement with the more stable *s*-trans conformer. With B3-LYP especially, the match is considerable better than for the *s*-cis form. In contrast to that with TDDFT/BH-LYP, the spectrum obtained for the *s*-cis conformer is more similar to the experimental spectrum so that one would incorrectly consider it to be more stable. Thus, only the TDDFT/B3-LYP method has the ability to predict the right conformer.

4. Conclusions

The aim of this methodical study was a critical evaluation of the ability of different quantum chemical methods to reproduce experimental electronic circular dichroism (CD) spectra. Two single-reference approaches (TDDFT and CC2) and two multireference methods (MRMP2 and DFT/MRCI) were considered and applied to a test suite of molecules with a wide variety of chromophores. One of our intentions was to test methods at their "limits", meaning that we selected very difficult "worst-case" systems. All of the methods have also been applied to three model systems where accurate ab initio MRCI reference data were used for comparison. To investigate the effect of exact HF-exchange mixing systematically, the TDDFT calculations were carried out with the BP86, B3-LYP ,and BH-LYP functionals. The TDHF method was included as an upper limit for the HF-exchange part of the functional.

The imbalanced description of Rydberg excited states compared to valence-type excited states or, in general, of states with different spatial dimension is a serious disadvantage of the TDDFT method. For example, dimethyloxirane shows that for Rydberg states of the same angular momentum but very different spatial dimension even a wrong ordering is predicted. These effects, which are also observed for the camphor derivatives and pinene, are attributed to the wrong asymptotic behavior of the DF potentials. Introducing hybrid functionals fixes the problem to a certain extent, but our investigations show that the optimum fraction of Hartree−Fock exchange changes in an unpredictable manner from system to system. By using HF(N-1) orbitals and a valence basis set augmented with a single set of diffuse functions, a balanced description of valence and Rydberg excited states can be achieved with the MRMP2 method. The CC2 approach allows the treatment of Rydberg states with ordinary AO basis sets such as aug-SV(P) with acceptable accuracy.

Molecules with inherently achiral chromophores turned out to be theoretically very demanding. The MRMP2 method especially, at least in its present (simplified) form, does not have the potential to account for the many weak contributions leading to CD in such molecules. This is mainly due to the rotatory strengths that are dominated by the (too small) reference CI expansion in the MRMP2 treatment. The performance of TDDFT is better in these cases but is still not satisfactory. For example, in camphor, the rotatory strength of the n $\rightarrow$ 3s transition is wrongly predicted by the B3-LYP or BP86 functionals whereas BH-LYP (and DFT/MRCI) gives the right answer. Also, the Cotton effects of the 3p states differ substantially in absolute value and sign depending on which functional is used. The fact that for the very similar norcamphor system a correct sign is obtained for the CD of the n $\rightarrow$ 3s transition with all functionals underlines the complexity of these systems.

An accurate description of Rydberg−valence mixed states represents a general problem in theoretical electronic spectroscopy but has special relevance in CD spectroscopy because of the greater sensitivity of the rotatory strengths with respect to changes in the wave functions. Incorrect Rydberg−valence mixing causes significant problems in α-pinene and dithiadecaline. In this context, we stress that the examination of model compounds can be helpful but cannot replace the investigation of real molecules. The results for H_2S_2 or ethylene are much better than those obtained for the corresponding real systems—dithiadecaline and pinene.

In molecules with extended delocalized π systems such as DMP and CBB, mixing among different valence states becomes important. Also, in these cases, we observe a substantial dependence of the results on the chosen functional used in TDDFT. An appropriate description of the higher-lying transitions in these large aromatic systems by CC2 and TDDFT is principally difficult because of the increased contribution of double and higher excitations. Therefore, the electronic nature and even the number of states are incorrectly predicted, especially by TDDFT. For the higher-energy regions, multireference methods are clearly superior, and in particular, the results obtained with the DFT/MRCI method are promising.

The performance for the transition-metal complex investigated is particularly bad. As observed previously,[16] CC2 is not at all applicable in this case, and perturbative methods such as our simplified MRMP2 ansatz also seem to have inherent problems. Furthermore, only with the B3-LYP functional is TDDFT able to reproduce the low-energy part of the spectra. However, to draw more definite conclusions about this class of compounds, further investigations of other systems with, for example, different metals and ligands are necessary.

The final conclusion of this work is that none of the methods performs reliably for all molecules in the test suite. A good description of the excitation energies provides in general no conclusion about the accuracy of the corresponding rotatory strengths. Methods providing accurate results for weakly disturbed, inherently achiral chromophores are limited to medium-sized molecules because of the high computational effort. The best overall performance is achieved by the DFT/MRCI and CC2 methods, although some "outliers" have also been observed here. The TDDFT method should be used carefully, especially for systems with diffuse or charge-transfer states. Out of the three functionals tested, the hybrid B3-LYP seems to perform the best, although in some systems a larger fraction of HF exchange is definitely necessary. In summary, we strongly recommend the simultaneous application of different complementary single and multireference methods that can indicate difficulties and thereby increase the reliability of the theoretical treatment.

On the positive side, we can conclude that the quality of most of the simulated spectra (except those from TDHF and some from TDDFT/BP86) is good enough to assign absolute configurations of chiral molecules with very high certainty in comparison to the experimental data. With further development of the quantum chemical methods, thereby increasing accuracy, the future for the solution of conformational problems with theoretical CD spectroscopy seems bright.

Acknowledgment. We are grateful to C. Mück-Lichtenfeld for his continuous support of our parallel PC cluster on which all calculations have been performed. This work was supported in part by the Deutsche Forschungsgemeinschaft through the SFB 424.

References and Notes

(1) Rauk, A. In *Encyclopedia of Computational Chemistry*; Schleyer, P. v. R., Ed.; John Wiley & Sons: New York, 1998.

(2) *Circular Dichroism*; Nakanishi, K., Berova, N., Woody, R. W., Eds.; VCH Publishers: New York, 1994.

(3) Lightner, D. A.; Gurst, J. E. *Organic Conformational Analysis and Stereochemistry from Circular Dichroism Spectroscopy*; Wiley-VCH: New York, 2000.

(4) Moffitt, W.; Woodward, R. B.; Moscowitz, A.; Klyne, W.; Djerassi, C. *J. Am. Chem. Soc.* **1961**, *83*, 4013.

(5) Scott, A. I.; Wrixon, A. D. *Tetrahedron* **1970**, *26*, 3695.

(6) Moscowitz, A.; Charney, E.; Weiss, U.; Ziffer, H. *J. Am. Chem. Soc.* **1961**, *83*, 4661.

(7) Grimme, S.; Harren, J.; Sobanski, A.; Vögtle, F. *Eur. J. Org. Chem.* **1998**, 1491.

(8) Furche, F. *J. Chem. Phys.* **2001**, *114*, 5982.
(9) Yabana, K.; Bertsch, G. F. *Phys. Rev. A* **1999**, *60*, 1271.
(10) Autschbach, J.; Ziegler, T.; van Gisbergen, J. A.; Baerends, E. J. *J. Chem. Phys.* **2002**, *116*, 6930.
(11) Hansen, A. E.; Bak, K. L. *Enantiomer* **1999**, *4*, 455.
(12) Casida, M. E.; Chong, D. P. In *Recent Advances in Density Functional Methods*; Chong, D. P., Eds.; World Scientific: Singapore, 1995; p 155.
(13) Christiansen, O.; Koch, H.; Jørgensen, P. *Chem. Phys. Lett.* **1995**, *243*, 409.
(14) Waletzke, M.; Grimme, S. *Phys. Chem. Chem. Phys.* **2000**, *2*, 2075.
(15) Grimme, S.; Waletzke, M. *J. Chem. Phys.* **1999**, *111*, 5645.
(16) Parac, M.; Grimme, S. *J. Phys. Chem. A* **2002**, *106*, 6844.
(17) Bauernschmidt, R.; Ahlrichs, R. *Chem. Phys. Lett.* **1996**, *256*, 454.
(18) Sala, F. D.; Görling A. *J. Chem. Phys.* **2001**, *115*, 5718.
(19) Casida, M. E.; Gutierrez, F.; Guan, J.; Gadea, F.-X.; Salahub, D.; Daudey, J.-P. *J. Chem. Phys.* **2000**, *113*, 7062.
(20) van Leeuwen, R.; Baerends, E. J. *Phys. Rev. A* **1994**, *49*, 2421.
(21) Furche, F.; Ahlrichs, R.; Wachsmann, C.; Weber, E.; Sobanski, A.; Vögtle, F.; Grimme, S. *J. Am. Chem. Soc.* **2000**, *122*, 1717.
(22) Newman, M. S.; Darlak, R. S.; Tsai L. *J. Am. Chem. Soc.* **1967**, *89*, 6191.
(23) Lightner, D. A.; Hefelfinger D. T.; Powers, T. W.; Frank, G. W.; Trueblood, K. N. *J. Am. Chem. Soc.* **1972**, *94*, 3492.
(24) Ahlrichs, R.; Bär, M.; Baron, H.-P.; Bauernschmitt, R.; Böcker, S.; Ehrig, M.; Eichkorn, K.; Elliott, S.; Furche, F.; Haase, F.; Häser, M.; Horn, H.; Hättig, C.; Huber, C.; Huniar, U.; Kattannek, M.; Köhn, A.; Kölmes, C.; Kollwitz, M.; May, K.; Ochsenfeld, C.; Öhm, H.; Schäfer, A.; Schneider, U.; Treutler, O.; Arnim, M. v.; Weigend, F.; Weis, P.; Weiss, H. TURBOMOLE, version 5.5; Universität Karlsruhe: Karlsruhe, Germany, 2002.
(25) Hättig, C.; Weigend, F. *J. Chem. Phys.* **2000**, *113*, 5154.
(26) Schäfer, A.; Huber, C.; Ahlrichs, R. *J. Chem. Phys.* **1994**, *100*, 5829−5835.
(27) Schäfer, A.; Horn, H.; Ahlrichs, R. *J. Chem. Phys.* **1992**, *97*, 2571−2577.
(28) Dunning, T. H. *J. Chem. Phys.* **1993**, *98*, 7059.
(29) Kendall, R. A.; Dunning, T. H.; Harrison, R. J. *J. Chem. Phys.* **1992**, *96*, 6796.
(30) Olsen, J.; Christiansen, O.; Koch, H.; Jørgensen, P. *J. Chem. Phys.* **1996**, *105*, 5082.
(31) Bauernschmitt, R.; Ahlrichs, R. *Chem. Phys. Lett.* **1997**, *264*, 573.
(32) Eichkorn, K.; Weigend, F.; Treutler, O.; Ahlrichs, R. *Theor. Chem. Acc.* **1997**, *97*, 119.
(33) Weigend, F.; Häser, M.; Patzelt, H.; Ahlrichs, R. *Chem. Phys. Lett.* **1998**, *294*, 143.
(34) Buenker, R. J.; Peyerimhoff, S. D. *Theor. Chim. Acta* **1974**, *35*, 33.
(35) Roos, B. O.; Andersson, K. *Chem. Phys. Lett.* **1995**, *245*, 215.
(36) Langhoff, S. R.; Davidson, E. R. *Int. J. Quantum Chem.* **1974**, *8*, 61.
(37) Rauk, A. *J. Am. Chem. Soc.* **1984**, *106*, 6517.
(38) Ha, T.-K.; Cencek, W. *Chem. Phys. Lett.* **1991**, *182*, 519.
(39) Pericou-Cayere, M.; Rerat, M.; Dargelos, A. *Chem. Phys.* **1998**, *226*, 297.
(40) Linderberg, J.; Michl, J. *J. Am. Chem. Soc.* **1970**, *92*, 2619.
(41) Bergson, G. *Ark. Kemi* **1958**, *12*, 233.
(42) Bergson, G. *Ark. Kemi* **1962**, *18*, 409.
(43) Dunning, T. H. *J. Chem. Phys.* **1989**, *90*, 1007.
(44) Bouman, T. D.; Hansen, A. E. *J. Chem. Phys.* **1977**, *66*, 3460.
(45) Liskow, D. H.; Segal, G. A. *J. Am. Chem. Soc.* **1978**, *100*, 2945.
(46) Breest, A.; Gödderz, K. H.; Ochmann, P.; Carnell, M.; Hormes, J. *Mol. Phys.* **1994**, *82*, 539.
(47) Carnell, M.; Grimme, S.; Peyerimhoff, S. D. *Chem. Phys.* **1994**, *179*, 385.
(48) Grimme, S. Unpublished work.
(49) Snatzke, G. *Angew. Chem.* **1979**, *91*, 380.
(50) Pulm, F.; Schramm, J.; Hormes, J.; Grimme, S.; Peyerimhoff, S. D. *Chem. Phys.* **1997**, *224*, 143.
(51) Vögtle, F.; Grimme, S.; Hormes, J.; Dötz, K.-H.; Krause, N. In *Final Report of the Sonderforschungsbereich "Wechselwirkungen in Molekülen"*; Peyerimhoff, S. D., Ed.; Wiley-VCH: New York, 2002.
(52) Mason, M. G.; Schnepp, O. *J. Chem. Phys.* **1973**, *59*, 1092.
(53) Neubert, L. A.; Carmack, M. *J. Am. Chem. Soc.* **1974**, *96*, 943.
(54) Laarhoven, H.; Prinsen, J. C. *Top. Curr. Chem.* **1983**, *125*, 63.
(55) Lightner, D. A.; Hefelfinger, D. T.; Powers, T. W.; Frank, G. W.; Trueblood, K. N. *J. Am. Chem. Soc.* **1971**, *94*, 3492.
(56) Platt, J. R. *J. Chem. Phys.* **1949**, *17*, 484.
(57) Armstrong, R. N.; Ammon, H. L.; Darnow, J. N. *J. Am. Chem. Soc.* **1987**, *109*, 2077.
(58) Birks, J. B. *Photophysics of Aromatic Molecules*; Wiley: New York, 1970.
(59) Harada, N.; Uda, H.; Nozoe, T.; Okamoto, Y.; Wakabayashi, H.; Ishikawa, S. *J. Am. Chem. Soc.* **1987**, *109*, 1661.
(60) Schmalz, H.-G. Unpublished work.
(61) He*β*ler, E.; Schmalz H.-G.; Dürner G. *Tetrahedron Lett.* **1994**, *35*, 4547.
(62) Klamt, A.; Schüürmann, G. *J. Chem. Soc., Perkin Trans. 2* **1993**, 799.